Measurement report: Changing characteristics of atmospheric CH_4 in the Tibetan Plateau: records from 1994 to 2019 at the Mount Waliguan station

Shuo Liu[1,2,3], Shuangxi Fang[3], Peng Liu[4], Miao Liang[5], Minrui Guo[6], Zhaozhong Feng[1,7]

[1]State Key Laboratory of Urban and Regional Ecology, Research Center for Eco-Environmental Sciences, Chinese Academy of Sciences, Beijing, China

[2]College of Resources and Environment, University of Chinese Academy of Sciences, Beijing, China

[3]College of Environment, Zhejiang University of Technology, Hangzhou, China

[4]Mt. Waliguan background station, China Meteorological Administration (CMA), Qinghai, China

[5]Meteorological Observation Center (MOC), China Meteorological Administration (CMA), Beijing, China

[6]College of Global Change and Earth System Science, Beijing Normal University, Beijing, China

[7]Key Laboratory of Agrometeorology of Jiangsu Province, Institute of Ecology, School of Applied Meteorology, Nanjing University of Information Science & Technology, Nanjing, China

Correspondence:

Shuangxi Fang (fangsx@cma.gov.cn); Zhaozhong Feng (zhzhfeng201@hotmail.com)

Abstract. A 26-year long-term record of atmospheric methane (CH_4) measured in-situ at the Mount Waliguan (WLG) station, the only WMO/GAW global station in inland Eurasia, is presented. Overall, a nearly continuous increase of atmospheric CH_4 was observed at WLG with a yearly growth rate of 5.1 ± 0.1 ppb yr^{-1} during 1994-2019, except for some particular periods with near-zero or negative values, e.g. 1999-2000, and 2004-2006. The average CH_4 mole fraction was only 1799.0 ± 0.4 ppb in 1994 but increased about 133 ppb and reached a historic level of 1932.0 ± 0.1 ppb in 2019. The case study in the Tibetan Plateau showed that the atmospheric CH_4 increased rapidly. During some special period, it is even larger than that of city regions (e.g. 6.7 ± 0.2 ppb yr^{-1} in 2003-2007). Generally, the characteristics of CH_4 varied in different observing periods: i) the diurnal cycle has been becoming apparent and the amplitudes of the diurnal or seasonal cycles increased over time, ii) the wind sectors with elevated CH_4 mole fractions switched from ENE-…-SSE sectors in early periods to NNE-…-E sectors in later years, iii) the area of source regions increased as the years progressed and strong sources shifted from northeast (city regions) to southwest (Northern India), iv) the annual growth rates in recent years (e.g. 2008-2019) were significantly larger than that in early periods (e.g. 1994-2007).

1 Introduction

Since the pre-industrial era, the emission of greenhouse gases (GHGs) has increased continuously and large increases have been found in recent years, with the concentration now being higher than ever (WMO, 2019). The GHGs perturb the infrared radiation balance, which traps the heat in the atmosphere and contributes to global warming, melting glaciers, extreme weather events and many other global climate changes (IPCC, 2014). The recent 30-year span from 1983 to 2012 was the warmest of the last 800 years in the Northern Hemisphere, and half of the rising surface temperatures were due to increased GHGs emissions (IPCC, 2014). As one of the most important GHGs, methane (CH_4) has a global warming effect that is just less than carbon dioxide (CO_2) (Etminan et al., 2016). CH_4 has an 8-12 year lifetime (Battle et al., 1996), with a global warming potential ~23 times greater than CO_2 over a 100-year horizon (Weber et al., 2019). CH_4 also contributed to about 17% of the radiative forcing caused by long-lived greenhouse gases was from 1750 to 2016 (Etminan et al., 2016). Since the beginning of the industrial era, the concentration of CH_4 rapidly increased because of the influence of anthropogenic activities (Saunois et al., 2016). Results from ice cores analyses in Antarctica showed that the atmospheric concentration of CH_4 reached a level unprecedented over the last 0.8 million years (IPCC, 2014).

At the beginning of the 1990s, the CH_4 mole fraction showed a decreasing trend. Consequently, the reverse trend has been observed since 1998 due to the higher global mean temperature (Dlugokencky et al., 1998; Nisbet et al., 2014). However, a low growth rate was sustained over 1999 to 2006, except for years with El Niño events (2002/2003) (Dlugokencky et al., 1998). The annual growth rate dropped from ~12 ppb yr^{-1} to near 0 from the late 1980s to 2006, followed by a renewed CH_4 increase since then (Nisbet et al., 2019). During 2007-2013, the annual growth rate of methane was 5.7 ± 1.2 ppb yr^{-1}. After 2013, the atmospheric CH_4 grew at rates not observed, such as 12.7 ± 0.5 ppb yr^{-1} in 2014 and 10.1 ± 0.7 ppb yr^{-1} in 2015 (Nisbet et al., 2016, 2019). In the most recent decade, the global mean growth rate was 7.1 ppb yr^{-1} (WMO, 2019).

The World Meteorological Organization/Global Atmospheric Watch Programme (WMO/GAW) annual greenhouse gas bulletin revealed that the global average mole fraction of CH_4 reached a new high with 1869 ± 2 ppb in 2018 (Rubino et al., 2019), which was ~259% of pre-industrial levels (~722 ppb around 1750 C.E. (Common Era)) (Etheridge et al., 1998; WMO, 2019).

Atmospheric CH_4 is mainly emitted from natural sources (e.g. about 40% from ruminants and wetlands) and anthropogenic sources (e.g. about 60% from paddies, cattle ranches, coal mines, fossil fuels, and biomass burning) (Hausmann et al., 2016; Saunois et al., 2016). Observations from the GAW indicated that the causes of the recent increase were likely attributed to anthropogenic emissions at mid-latitudes in the Northern Hemisphere and the wetlands in the tropics (WMO, 2019). The rapid development of population growth, economic expansion, and urbanization of countries has led to more and more fossil fuel production and consumption (e.g. the large-scale exploitation of natural gas, oil, and coal) and biomass burning. Consequently, large amounts of anthropogenic CH_4 were emitted around the world in recent years (Galloway, 1989; Streets and Waldhoff, 2000; Wang et al., 2002; Lin et al., 2014; Hausmann et al., 2016). The recent carbon isotope study revealed that biogenic emissions might also have driven CH_4 increases, including microbial sources from rice, paddies, ruminants, termites, enteric fermentation, or a combination of these (Nisbet et al., 2016; Schaefer et al., 2016; Wolf et al., 2017). About 90% of the CH_4 destruction in the atmosphere is from the reaction with hydroxyl radicals (·OH) (Vaghjiani and Ravishankara, 1991; Bousquet et al., 2011), an important oxidant in the troposphere (Logan et al., 1981). Therefore, the inter-annual variation of ·OH or the decline of the oxidative capacity of the atmosphere may also cause the recent increase in the CH_4 growth rates (Rigby et al., 2017; Turner et al., 2017). The exact causes of significant increase in the CH_4 emissions in past years remain debated, especially for the anomalous periods with a suddenly large growth, due to the sparse time and space measurements and the crude models, which limited our understanding of the global

variation of atmospheric CH_4 (Saunois et al., 2019; Weber et al., 2019). As a consequence, it will be impractical to predict CH_4 trends in the future, and then to develop realistic management (Nisbet et al., 2019).

Systematic observations are a prerequisite to get an accurate understanding of the spatial and temporal behaviors of atmospheric CH_4 concentrations. Since 1978, systematic measurements of atmospheric CH_4 have been taken around the world (Blake et al., 1982; Rasmussen and Khalil, 1984; Dlugokencky et al., 1994). On the northern slope of the Mauna Loa volcano, Hawaii, there exists the first global station, Mauna Loa (MLO), which has performed at about 3397m above sea level (a.s.l.) and far away from local sources and sinks. It has the longest record of continuous atmospheric CH_4 observation (Keeling et al., 1976). Recently, other stations have been installed for CH_4 observation, such as the Barrow (BRW), South Pole (SPO) (polar site) (Dlugokencky et al., 1995), Cape Grim (CGO) and Minamitorishima (MNM) (coastal/island sites) (Pearman and Beardsmore, 1984; Wada et al., 2007), Jungfraujoch (JFJ) and Mount Waliguan (continental mountain site) (Zhou et al., 2004; Loov et al., 2008). Hundreds of CH_4 observation stations worldwide are currently running under the framework of the WMO/GAW.

China has the largest anthropogenic CH_4 emissions in the world (Janssens-Maenhout et al., 2019). The Qinghai-Tibetan Plateau with an average altitude of over 4000m a.s.l. has long been recognized as the roof of the world. By coincidence, the two largest CH_4 source regions in the world (i.e. Eastern China and Northern India) are trapped by the Tibetan Plateau in between (Zhang et al., 2011; Fu et al., 2012; Wilson and Smith, 2015). Under the characteristics of special geographical conditions, lower population density, rare industrial activities, and high sensitivity to external disturbances, the Tibetan Plateau is one of the ideal regions to observe a continual CH_4 signal (Zhou et al., 2005; Fu et al., 2012; Zhang et al., 2013). Most of the previous studies reported on the short-term CH_4 variations in China and concluded that the long-term observation is of great value to enhance the understanding of the global carbon

cycle (Cai et al., 2000; Zou et al., 2005; Wang et al., 2009; Fang et al., 2013; Yuan et al., 2019). As the rapid development of China and India continues, the characteristics of CH_4 on the Tibetan Plateau, might change significantly over time. Since 1994, in-situ measurements of atmospheric CH_4 have been launched at the Mt. Waliguan (WLG) station. To study the long-term variations of the atmospheric CH_4 and get a new insight on its characteristics in the inland of Eurasia, the performance of a 26-year of in situ observations at the Mt. Waliguan baseline observatory were evaluated, which is the longest record in China. Temporal patterns, annual variations, long-term trends, air mass transports, and the spatial distribution of potential sources were analyzed. In addition, the case studies combining atmospheric carbon monoxide (CO) measurements and a separate analysis between the Tibetan Plateau and the city regions were performed to constrain the contribution of anthropogenic emissions.

2 Methodology

2.1 Measurement site

The Mt. Waliguan (WLG, 36.28° N, 100.09° E, 3816m a.s.l.) station is situated at the edge of northeast Tibetan (Qinghai-Xizang) Plateau, which is in remote western China and isolated from populated and industrial regions (Fig. 1). WLG is the only WMO/GAW global background station in Eurasia and is run by the China Meteorological Administration (CMA). The surrounding of the site are pristine with sparse vegetation, naturally arid and semi-arid grasslands. Small farms with yak and sheep are in the valley. Two adjacent large cities Xining (~2.2 million populations) and Lanzhou, are located about 90 km northeast and 260 km east of the station, respectively. The Longyangxia hydroelectric station (~380 km^2) is located approximately 13 km south to southwest of WLG. The predominant winds at WLG are mainly from southwest and east in winter and summer, respectively (Zhou et al., 2004; Zhang et al., 2011), which is controlled by Tibetan Plateau monsoon. Simultaneously, diurnal

147 variations of vertical winds at WLG are influenced by mountain-valley breezes, where
148 upslope flow brings heated air masses from the boundary layer to the site in daytime
149 and downslope flow results in cool air masses transport from the mountain peak to the
150 site. Under this unique location, the observation at WLG can obtain essential
151 information on CH_4 sources and sinks from Eurasia (Zhou et al., 2005; Zhang et al.,
152 2013).
153
154 **2.2 Instrumental setup**

155 Atmospheric CH_4 has been measured quasi-continuously using a HP 5890 gas
156 chromatograph (GC) equipped with a flame ionization detector (FID) since July 1994,
157 and an Agilent 6890N GC equipped with a FID since June 2008. Both of the systems
158 used the same sampling procedures. A Cavity Ring Down Spectroscopy system (Picarro
159 G1301) began in January 2009 and the instrument was upgraded to Picarro G2401 in
160 2015. Ambient air is delivered to the above systems at about 5 L/min by a KNF
161 Neuberger N2202 vacuum pump via a dedicated 0.95 cm o.d. sample line from an 80m
162 intake line attached to an 89m steel triangular tower located approximately 15m from
163 the main observatory. The residence time of the ambient air from the top of the tower
164 to the instrument is 30 s. The ambient air is first passed through a 7 mm stainless steel
165 membrane filter located upstream of the pump and then (after the pump) passed through
166 a pressure relief valve set at 1 atm to release excess air and pressure. The ambient air is
167 then dried to a dew point of approximately -60°C by passing it through a glass trap
168 submerged in a -70°C methanol bath. All standard gases supplied to the instruments are
169 from pressurized 37.5 L treated aluminum alloy cylinders fitted with high-purity, two-
170 stage gas regulators. Stainless steel tubing (0.32 cm o.d., 0.22 cm i.d.) is used for the
171 standard gas sample line and the ambient sample line after the cold trap. An automated
172 sampling module equipped with a VICI 8 ports valve is designed to sample from
173 separate gas streams (standard tanks and ambient air). According to the comparability
174 target of WMO/GAW program (WMO, 2019), methane mole fractions are referenced

to a Working High standard (WH) and a Working Low standard (WL). Additionally, a calibrated cylinder filled with compressed ambient air is used as a Target gas (T) to check the precision and stability of the system routinely. Diagram of the observing system during different periods could be seen at Zhou et al. (2004) and Fang et al. (2013). Here, we focus on the longest continuous measurements of CH_4 from August 1994 to December 2019 at WLG. Data gaps in limited periods are because of the malfunction of instrument and the maintenance of the sampling system.

The records of CO in this study was initinially observed by an RGA-3 gas chromatograph (GC) equiped with an HgO reduction detector (Trace Analytical Inc.) since 1994. An automated sampling module was designed to sample from ambient air and a series 9 standards. Deailed diagram of the system was described by Zhang et al. (2011). Since 2010, the CO has been measured by the Cavity Ring Down Spectroscopy instrument (Picarro G1302 and G2401 since 2015). The scale for all of the CO measurement were further updated to WMO X2014A.

2.3 Data processing

Most on-site CH_4 observations were unavoidably influenced by local sources and other complex conditions (e.g. traffic transportation, various topography). As a result, the records cannot fully represent the regional atmospheric CH_4 in well-mixed conditions (Liu et al., 2019). To get regionally representative records, we excluded the CH_4 data influenced by local sources adjacent to the site (e.g. agricultural fields, cities, traffic emissions). The hourly CH_4 data were classified as Locally/Regionally representative through the meteorological approach, which was based on essential meteorological information, similar to previous studies by Zhou et al. (2004) and Liu et al. (2019). In this study, the CH_4 records associated with local surface winds from selected sectors, i.e. NNE-…-ENE in spring, NE-…-SE in summer, NE-…-ESE in autumn, and NE-ENE in winter, were flagged as locally influenced (27.0%). Subsequently, we rejected portion of daytime records to minimize the effect of human activities (16.9%), e.g. 9:00-

13:00 LT (local time) in summer, and 10:00-17:00 LT in winter. Finally, we filtered CH_4 data into locally influenced when the surface wind speeds were less than 1.5 m s^{-1} to minimize the very local accumulation (9.2%).

In order to investigate the influence of anthropogenic emissions from cities and remote area as Tibetan plateau, we divided the CH_4 data into two main influencing regions according to the analysis, including the geographical conditions, the effect of surface winds, the long-range transports, and the potential source distributions. The first region covers the northeast and southeast (NNE-…SE) of WLG, which is denoted as City Regions (CR). The second region is located the south to west (S-…-W) of the station and is well known Tibetan (Qinghai-Xizang) Plateau (TP) (Fig. S1). Accordingly, the hourly CH_4 records when the surface winds coming from these sectors were divided into two subsets (i.e. TP and CR). The long-term variations between the two regions as well as the total regional time series were further compared and analyzed.

To understand the influence of local surface wind, hourly CH_4 data was binned into 16 horizontal wind direction classes (Fang et al., 2013). In this study, we used the 'polarPlot' function in the 'openair' package of the statistical software R (R Core Team, 2020). It shows the bivariate (i.e. wind speed and wind direction) polar plot of CH_4 concentrations, and the concentrations are calculated as a continuous surface by modelling using smoothing techniques (Carslaw et al., 2006; Diederich, 2007). Also, conditional probability function (CPF) was used to investigate the probability of which wind directions are dominated by high CH_4 mole fractions (Uria-Tellaetxe and Carslaw, 2014). In order to study the pollution transport pathways of air masses at WLG, the cluster analysis of 3 days back trajectories was applied using the Hybrid Single-Particle Lagrangian Integrated Trajectory (HYSPLIT) dispersion model (Draxier and Hess, 1998; Rousseau et al., 2004) on the strength of gridded meteorological data (2004-2017) from the National Oceanographic and Atmospheric Administration's Air Resources Laboratory (NOAA-ARL). The spatial resolution of the model is 0.5×0.5

231 degree and the model height is 10 km a.s.l. We computed the back trajectories
232 coincident with hourly CH_4 mole fractions. The trajectories for January, April, July and
233 October, were calculated to represent the seasons of winter, spring, summer and
234 autumn, respectively. The spatial source distributions of annual CH_4 were analyzed
235 using the Potential Source Contribution Function (PSCF) approach, which computed
236 the conditional probability of the residence times of air parcels with greater
237 concentration than threshold transport to the exact receptor site (Ashbaugh et al., 1985).
238 In this study, PSCF value was calculated in 0.5×0.5-degree grid cell (*i*, *j*):

239 $$\mathrm{PSCF}_{ij} = m_{ij} / n_{ij} \quad (1)$$

240 n_{ij} represents the number of endpoints that terminate in the *ij*th grid cell, while the
241 number of trajectories with concentration exceed the threshold value was defined as m_{ij}
242 (Polissar et al., 1999). In order to reduce the abnormal influence of small n_{ij} values in
243 some grid cells, PSCF_{ij} was further computed by an arbitrary weighting function W_{ij} as
244 below.

245 $$W_{ij} = \begin{cases} 1.00 & 3n_{ave} < n_{ij} \\ 0.70 & 1.5n_{ave} < n_{ij} \le 3n_{ave} \\ 0.42 & n_{ave} < n_{ij} \le 1.5n_{ave} \\ 0.05 & n_{ij} \le n_{ave} \end{cases} \quad (2)$$

246 W_{ij} represents the weight of cell (*i*, *j*), n_{ij} is the number of trajectory endpoints that fall
247 in the *ij*th grid cell, while the n_{ave} shows the mean number of the endpoints in all grid
248 cells.

249 In order to fill the data gaps so as to evaluate the long-term CH_4 trend, we applied
250 the curve fitting approach by Thoning et al. (1989). We also calculated the trend curve
251 that excluded the influence of seasonal variation, and then got the annual growth rates
252 by the average of the first derivative of the trend curve. The function consists of the
253 polynomial part and the annual harmonics part:

254 $$f(t) = a_0 + a_1 t + a_2 t^2 + \cdots + a_{(k-1)} t^{(k-1)} + \sum_{n=1}^{nh} c_n [\sin(2n\,\pi\, t) + \varphi_n] \quad (3)$$

255 'k' represents the number of polynomial part. 'nh' is the number of harmonics part. We

applied k = 3 polynomial terms (a quadratic) for multi-year trends and nh = 4 yearly harmonics for seasonal cycles in this study. The fast Fourier transform (FFT) was utilized to smooth the fitting residuals (Press et al., 1992).

The significant difference test was applied by the 'scheirerRayHare' function in the 'rcompanion' package of R software, which is a non-parametric test for two-way ANOVA analysis. The multiple comparison was used by Wilcoxon rank sum test with R (R Core Team, 2020). For the correlation analysis between CH_4 and CO, we obtained the detrended time series of CH_4 and CO from 2004-2017 based on the method by Thoning et al. (1989). The detrended values are denoted as ΔCH_4 and ΔCO, which are the original data points minus the trend curve. To accurately obtain the correlation slopes of ΔCO and ΔCH_4, i.e. $\Delta CO/\Delta CH_4$, a rolling linear regression was applied to the ΔCH_4 and ΔCO time series by the 'roll_lm' function in 'roll' package of R (R Core Team, 2020). We successively moved a 24-h time window by 1 h over the whole time series. Similar to the study by Tohjima et al. (2014), we set three criteria to achieve a better quality control of the slopes. When (i) the number of CH_4 record is less than five in 24 hours, (ii) the coefficient variation of the correlation slope is more than 15%, (iii) the absolute value of the correlation slope is less than 0.8 ($|R| < 0.8$), the correlation slopes were identified as statistically insignificant and inaccurately and were rejected. In order to understand the year to year variations, we analyzed the CH_4 variation over different periods in 1994-2019. The entire CH_4 time series were divided into five observing periods, i.e. 1994-1997, 1998-2002, 2003-2007, 2008-2012, and 2013-2019, according to the significant stages or the critical time period of atmospheric CH_4 variations from previous studies (Zhou et al., 2004; Fang et al., 2013; Zhang et al., 2013; Nisbet et al., 2019; WMO, 2020). Unless special notes, the average values in this study are presented with 95% confidence intervals (CIs).

3 Results and discussion

3.1 Extracting the regional atmospheric methane

To precisely understand the characteristics of atmospheric CH_4, including seasonal cycles and long-term trends, it is vital to identify the CH_4 records in well-mixed air without local contaminations (Liu et al., 2019). In this study, hourly CH_4 measurements between 1994 and 2019 were analyzed, resulting in 64.0% of the CH_4 data being classified as regionally representative, with an average CH_4 mole fraction of 1865.8 ± 0.4 ppb. The average of the locally influenced data (1868.2 ± 0.3 ppb) was larger than that of the regionally representative records (Table 1). The filtered regional/local time series was shown in Figure 2. It can be seen that the CH_4 mole fractions increased from 1994 to 2019. The atmospheric CH_4 showed a strong growth and displayed large fluctuation. In 1994, the average CH_4 mole fraction was only 1799.0 ± 0.4 ppb, however, the average value increased 133 ppb by the year 2019 (1932.0 ± 0.1 ppb) (Table 2). Compared with the global average mole fractions in recent years, i.e. 1853 ± 2 ppb in 2016, 1859 ± 2 ppb in 2017, and 1869 ± 2 ppb in 2018 (WMO, 2019; 2020), the atmospheric CH_4 mole fractions at WLG were significantly higher. These results indicated that WLG was affected by strong CH_4 sources in recent years, which were possibly due to the influence of the two largest source regions of Northern India and Eastern China (Fang et al., 2013; Zhou et al., 2004).

3.2 Diurnal variations

Distinct diurnal cycles were observed in four seasons during 1994-2019 at WLG. The CH_4 mole fraction increased from early morning, reached a maximum at noon, and had a trough in the late afternoon (Fig. 3f). However, differences also existed in four seasons. In spring and summer, the atmospheric CH_4 increased from 9:00 to 13:00 LT at noon, with a daily amplitude of 5.8 ±2.8 and 4.4 ± 3.4 ppb, respectively (Table S1). In autumn, the diurnal variation showed an amplitude of 4.3 ± 3.1 ppb with one peak at

noon. In winter, a large increase of CH_4 was found during 9:00-17:00 LT, with the largest peak to trough amplitude of 7.1 ± 2.9 ppb. Different patterns for diurnal CH_4 cycles were also found over different periods. In 1994-2002, the CH_4 mole fractions in the winter were higher than the other seasons (Fig. 3a-b), which was likely due to the manner of heating (e.g. large biomass burning) as well as the adverse diffusion conditions in cold weather (Fang et al., 2013). However, the highest value was found in summer during the periods of 2003-2007, 2008-2012, and 2013-2019 (Fig. 3c-e), which could be ascribed to the transport of anthropogenic emissions (e.g. southeast cities) by the meteorological factors (Zhang et al., 2013). Additionally, in summer, the intense herding or grazing activities around WLG have enhanced the regional CH_4 emissions and hence contributed to the higher CH_4 mole fractions (Zhou et al., 2004).

Similar to the previous studies by Zhang et al. (2013) and Fang et al. (2013), diurnal cycles were ambiguous before 2002 (Fig. 3a-b), but significant diurnal variations appeared afterward (Fig. 3c-e), which indicated that the local sources were weak at WLG in the past. The apparent diurnal cycles after 2002 may be attributed to the intense activities by humans (e.g. grazing, burning fuel), which were enhanced in the daytime and weakened at nighttime (Fang et al., 2013). The peak to trough amplitude almost increased in almost all seasons. For example, in spring the amplitude was 6.5 ± 3.1, 4.7 ± 2.1, 5.6 ± 2.7, 7.0 ± 3.1, and 6.9 ± 3.1 ppb over the periods of 1994-1997, 1998-2002, 2003-2007, 2008-2012, and 2013-2019, respectively (Table S1). The meteorological conditions (e.g. diffusion and transport) could have also contributed to the increasing CH_4 amplitude. WLG was remote from the populated center, therefore, the good diffusion conditions in the daytime may have brought high anthropogenic emitted CH_4 to the site. The increasing amplitude and CH_4 mole fractions suggested that WLG was increasingly affected by local and regional anthropogenic sources, such as gas exploitation, and grazing (Zhou et al., 2004).

3. 3 **The impact of local surface winds**

Similar to the short-term study by Zhou et al. (2004), the atmospheric CH_4 at WLG was significantly influenced by local surface winds from the northeast and southeast sectors (Fig. 4f). Slight differences were also found among seasons. In the spring, when the wind was originating from the NNE-NE-ENE-E sectors, the atmospheric CH_4 was enhanced by 8.0-15.4 ppb as compared to the seasonal average (1862.4 ± 3.7 ppb). In the summer and autumn, the wind from the NNE-NE-ENE-E-ESE-SE produced higher CH_4 mole fractions, with an enhancement of 2.5-14.6 ppb and 1.6-19.3 ppb, respectively. In winter, similar to that in spring, the CH_4 mole fractions significantly increased from NNE-NE-ENE-E sectors, with a value of 14.7-25.8 ppb higher than the seasonal average (1871.3 ± 6.7 ppb). In summer, the prevailing winds were from the NE-…-ESE sectors (~46%) (Fig. S2), and the CH_4 mole fractions were also higher in the related sectors. However, in autumn and winter, although the prevailing wind and the high wind speed were from SSW-…-W sectors (~ 40-50%) (Fig. S2), the high CH_4 mole fractions were from the opposite wind sectors of NNE-….-ESE (Fig. 4f), suggesting that strong local sources were distributed from northeast to southeast of WLG (city regions), and even covered the emission of natural sources. Causes of the elevated CH_4 from these sectors could be attributed to the large plantations of highland barley as well as the high population density in those areas (Fang et al., 2013). The two largest cities of Xining (with population of ~2.2 million) and Lanzhou (with population of ~4 million) are also situated in the northeast and east of WLG, respectively. The heavy human activities from anthropogenic fossil combustion, landfills, and livestock, could have also emitted large amounts of CH_4. Based on the data from the Emissions Database for Global Atmospheric Research (EDGAR), the increase of CH_4 emission was 500 kg yr^{-1} in these two regions throughout 1994-2015 (Crippa et al., 2019). Also, the Yellow River Canyon industrial area (YRC), which is ~500 km northeast of WLG, may also have contributed to the high CH_4 values (Zhou et al., 2003). With the rapid development of land-use, water utilization, and agriculture sources in the YRC, large

CH_4 emissions could have easily transported to WLG. Previous studies on black carbon (BC) and carbon monoxide (CO) also revealed that the high CH_4 values at WLG in winter were a result of transport from the YRC (Tang et al., 1999; Zhou et al., 2003).

The wind-rose distribution of CH_4 mole fractions indicated that the elevated CH_4 mole fractions varied in early periods (i.e. 1994-1997 and 1998-2002) to recent periods (2003-2007, 2008-2012, and 2013-2019). The elevated CH_4 was predominately from the ENE-..-SSE sectors in the early years (Fig. 4a-b) but evolved to the NNE-NE-ENE-E sectors in later years (Fig. 4c-e). Furthermore, the amplitude of enhancements was also increasing along with the progression of time. For example, in autumn, the maximums were from the E in 1994-1997, ENE in 1998-2002, ENE again in 2003-2007, NE in 2008-2012, and finally ENE in 2013-2019, with the successive increases of 8.6, 12.1, 14.7, 16.8, and 18.8 ppb, respectively. Therefore, the local surface wind from the city regions had an increasing effect on the atmospheric CH_4 at WLG.

The CPF was applied to hourly CH_4 and CO data by considering intervals of entire data percentiles including 0-20th, 20th-40th, 40th-60th, 60th-80th, and 80th-100th to draw the CPF polar plot (Uria-Tellaetxe and Carslaw, 2014). It was clear that the different sources only affected the CH_4 mole fractions in different percentile ranges (Fig. 5), meaning that the specific sources were prominent for specific percentile ranges. For most wind speed-directions, the CPF probability of the CH_4 being greater than the 60th percentile was trending to zero, and most sources contributed to the percentiles less than the 60th for the CH_4 mole fraction (e.g. 40th-60th). These results implied that most areas around WLG had a small contribution to the CH_4 emissions. In addition, the wind from the northeast and the southeast was important for the cases of the higher percentiles, resulting in the highest CH_4 mole fractions of 1870-1907 ppb for the 60th-80th percentiles and 1872907-2051 ppb for the 80th-100th percentiles (Fig. 5), which revealed the existence of a northeastern and a southeastern strong source region. The anthropogenic emissions from cities (e.g. Lanzhou or Chengdu) were the only cause for high values in the southeast. It’s obvious that the CO sources gradually shifted with the

increase of the percentile ranges (Fig. 5). The areas where the CPF probabilities were higher were to the NW-SW sectors when percentages ranged from 0 to 40. Nevertheless, when data exceeded the 60th percentile, the high probability areas completely moved to NE-SE sectors. Similar to that of CH_4, the high CO mole fractions were consistent from the east regions (urbanized areas) (Fig. 5), indicating strong anthropogenic sources in the city regions (e.g. Xining and Lanzhou) (Zhang et al., 2011).

3.4 Long-range transport and potential source distributions

3.4.1 Air mass transports

Figure 6 illustrates the cluster analysis of the 3-day back trajectories between 2004 and 2019. In the spring, majority of the air masses were from the west and northwest regions, which accounted for about 36.2% (cluster 3) and 36.4% (cluster 1) of the total trajectories (Fig. 6a). These air masses were accompanied by lower CH_4 mole fractions than those from the east and northeast regions, such as cluster 2 (27.3% of total) (Table 3). The largest enhancement was also in cluster 2 at ~6 ppb relative to the average. In the summer, 43.3% of the air masses were from eastern regions (cluster 3). However, the highest CH_4 mole fractions were in cluster 2 from northwest regions (Fig. 6b). The air masses from east and northeast regions passed over the cities of Xining and Lanzhou (capital of Gansu province), which are the populated centers and industrial areas, hence high CH_4 mole fractions were found. However, the higher CH_4 mole fractions were also observed when the air masses were from the northwest to southwest (Table 3), which were because the air masses had passed through the northwest of the Qinghai province and the central area of the Xinjiang Uygur Autonomous Region (XUAR). This is where the Ge'ermu urban area (the second largest city of Qinghai) was located and where there was with rapid industrial development, natural gas and petroleum resource exploitation, and residue burning of large crops, hence the CH_4 emissions were strong

(Fang et al., 2013; Zhang et al., 2013). In the autumn, all the air masses were originated from the west and northwest regions (Fig. 6c). In winter, the air masses primarily came from northwest and southwest regions, e.g. cluster 3 (56.4%), and cluster 1 (32.1%) (Fig. 6d), but the air masses (cluster 2) from city regions brought the highest CH_4 mole fractions with an enhancement of ~27 ppb over the seasonal average. Almost all the air masses were from the southwest or northwest regions in the autumn and winter, suggested these regions that were farther away from the site became strong source contributors to WLG.

3.4.2 Spatial distribution of potential source regions

The potential sources were analyzed over different periods, i.e. 2004-2007, 2008-2012, and 2013-2019 (Fig. 7). Generally, the strongest sources were located northeast or southeast of the station, especially in summer, but a large area of sources was identified from the southwest to the northwest regions, which also contained CH_4 emissions from the northwest Gansu province, the northwest Qinghai province and the southeast of the XUAR. Additionally, the source regions differed in various seasons. The potential source regions in the spring (Fig. 7a-c) and winter (Fig. 7j-l) were larger than those in the summer (Fig. 7d-f) and autumn (Fig. 7g-i). The seasonal difference was due to the effect of westerlies or the southeast monsoons (Zhou et al., 2004).

There were also trends in the CH_4 source regions correlated with specific years: i) the area of the potential source regions was increasing over time, and ii) the location of strong sources changed along with the time. For example, in autumn and winter, the CH_4 sources were very strong in the southeast and northeast regions during 2004-2007 (Fig. 7g & i), and then weakened in 2008-2012 (Fig. 7h & k). Finally, from 2013-2019 the sources almost moved to the southwest with a very large distribution area (Fig. 7i & l). More CH_4 sources appeared at WLG along with the progression of time, which could have been attributed to the influence of human expansion. The pattern of strong sources moving indicated that the southwest area relative to WLG, e.g. Northern India,

was gradually becoming a strong CH_4 contributor. India with abundant cattle as well as an extensive large-scale coal mining operation possibly contributed large amounts of CH_4 to move from northern India to the northeastern Tibetan Plateau (Fig. 7i & l) (Fu et al, 2012). The analysis of air mass transport (Fig. 6d) also supported the conclusions that the air masses from the southwest regions contributed the highest CH_4 mole fractions. The studies of atmospheric Hg at WLG by Fu et al. (2012) also supported this phenomenon, which found the long-range transport of atmospheric Hg from India to the Northeastern Tibetan Plateau.

3.5 Correlation analysis between CH_4 and CO

Because parts of the CH_4 and CO in atmosphere were from the same anthropogenic sources (e.g. fossil fuel combustion), the long-term trend of $\Delta CO/\Delta CH_4$ was helpful to understand the variation in the sources/sinks in many studies (Buchholz et al., 2016; Niwa et al., 2014; Tohjima et al., 2014; Wada et al., 2011). In this study, the hourly CO data from 2004 to 2019 was used to further analyze the long-term variations of CH_4 (Fig. S3). The regression slopes of $\Delta CO/\Delta CH_4$ from 2004 to 2019 were analyzed (Fig. S4). Figure 8 presents the seasonal cycles of the $\Delta CO/\Delta CH_4$ slopes. Generally, the slopes were larger in summer and smaller in winter during the observing period, except for 2004-2007 where the highest slope was in autumn. This was primarily due to the effect of monsoons and air mass transport. Tohjima et al. (2014) found an opposite variation at the Hateruma Island, which showed small slope values in the summer. Wada et al. (2011) analyzed more than 10-year seasonal variation of the $\Delta CO/\Delta CH_4$ ratios at three monitoring stations, i.e. MNM, Yonagunijima (YON), and Ryori (RYO) in Japan, which also showed an opposite trend to that of WLG. It was because these sites were considerably affected by the Asian continental source regions, where had enhanced emissions of CH_4 in the summer (rice paddies) and CO in the winter (fuels combustion). At WLG, Regional polarization in the concentration ratios of CH_4 and CO were seen (Fig. S5), which implied different strong source distributions between CH_4 and CO. In

the summer, the source emissions were mainly from the east-southeast regions (cities) with large amounts of CO but relatively lower CH_4, leading to the largest $\Delta CO/\Delta CH_4$. In contrast, the sources mostly from southwest-west regions (Tibetan Plateau) emitted large amounts of CH_4 but with relatively lower CO in the winter (Fang et al., 2013; Zhang et al., 2013). Hence, the opposite two air mass transports and source emissions led to a peak in $\Delta CO/\Delta CH_4$ in the summer and a trough in the winter (Fig. 8). These results revealed different local sources/sinks, the special topography conditions and source distributions around WLG.

The $\Delta CO/\Delta CH_4$ slopes showed large fluctuations from 2004 to 2019 at WLG (Fig. 9). The slopes showed a decreasing trend during 2004-2007 but then increased from 2007-2010, and decreased again after 2010. In 2007, a large increase in ΔCH_4 appeared, and from 2010 to 2013, the ΔCO decreased significantly (Fig. S4). Before 2010, large air masses and potential source regions were identified in eastern regions (cities) with the highest CO emission (Fig. 7 and Table 3). After 2010, the southwest regions had the highest CH_4 emissions but relatively low CO emissions. Therefore, the strong seasonal variation of $\Delta CO/\Delta CH_4$ also revealed that WLG was affected by different anthropogenic sources, e.g. sources from cities, and sources from the Tibetan Plateau, during a year, especially in the summer and winter. The long-term trend of the slopes implied that the source emission types (CO sources or CH_4 sources) around WLG might have been changing with human activities, like straw burning, in the early years, or coal mining in recent years.

3.6 Variation of long-term records

3.6.1 Seasonal cycles

Overall, the seasonal averages of regionally representative CH_4 at WLG were almost in a cycle starting with summer (1861.7 ± 0.4 ppb), then winter (1856.7 ± 0.3 ppb), autumn (1855.9 ± 0.4 ppb), and spring (1853.1 ± 0.3 ppb), except during 1994-1997 where there

was a maximum in the winter and a minimum in the autumn (Fig. 10). Seasonal averages in the CR were slightly different from that in the TP and even the total regional data. The seasonal averages in the TP were mostly higher than that in the CR from 1994 to 2019, except for in the winter (Table S2). The maximum mole fractions were mostly found in August and the minimum mole fraction appeared in April for the total regional time series, with a seasonal amplitude of 14.4 ppb. The peak to trough amplitude in the CR (~16.7 ppb) was higher than that in the TP (~15.1 ppb) during 1994-2019. The seasonal variations were consistent with the previous short-term studies from 2002-2006 at WLG (Zhang et al., 2013). However, these variations were almost opposite to observations at the adjacent stations of Lin'an, Shangdianzi, and Longfengshan in China (Fang et al., 2013, 2016). For other regional sites in the Asia, Guha et al. (2018) studied seasonal variability at the Sinhagad (SNG) and Cape Rama station (CRI) over India, which also showed an opposite trend to WLG due to the strong impact of monsoon dynamics. Ahmed et al. (2015) found that the seasonal CH_4 showed a maximum in the winter and a minimum in the spring at two urban sites of Guro (GR) and Nowon (NW), in Seoul, Korea over 2004-2013. Kim et al. (2015) investigated the decadal variation (1991-2013) of CH_4 at the East Asian sites, e.g. Ulaan Uul (UUM) in Mongolia and Tae-ahn Peninsula (TAP) in Korea, which revealed again an opposite seasonal trend to that of WLG.

The data were further compared with similar WMO/GAW global stations in the Northern Hemisphere, including MLO (19.54° N, -155.58° E, 3397m a.s.l.) (Dlugokencky et al., 1995, 2019a), JFJ (46.55° N, 7.99° E, 3580m a.s.l.) (Zellweger et al., 2016), MNM (24.29° N, 153.98° E, 7.1m a.s.l.) (Matsueda et al., 2004; Tsutsumi et al., 2006), as well as the marine boundary layer (MBL) from the NOAA/ESRL lab at a similar latitude (Dlugokencky et al., 2019b). It was seen that the stations in the Northern Hemisphere and the MBL showed an opposite trend to WLG with the minimum being in summer and maximum in the winter or spring (Fig. 11). The peak in the summer at WLG was attributed to larger grazing, human activities, ruminants, and easterly winds

coming from neighboring areas over other seasons. The CH_4 emissions from yaks and other ruminants in the Tibetan Plateau (alpine pasture) were very strong in the summer, preceded only by paddy emissions (Fang et al., 2013; Zhang et al., 2013). Furthermore, the dynamic transport by airflow from the polluted northeast/southeast region was also strong in summer, which all induced high CH_4 mole fractions and consequently an opposite trend than other sites (Ma et al., 2002; Xiong et al., 2009).

The seasonal amplitude at WLG (~14 ppb) was significantly lower than many other sites in the Northern Hemisphere, by about 35-70 ppb. Such sites included MLO in America, BRW in North Pole, UUM in Mongolia, TAP in Korea, Ny-Ålesund in Norway, Bialystok in Poland, Ochsenkopf in Germany, and Beromunster in Switzerland (Dlugokencky et al., 1995; Kim et al., 2015; Morimoto et al., 2017; Thompson et al., 2009; Popa et al., 2010; Satar et al., 2016). MBL also showed a larger amplitude than WLG (Fig. 11). The study at the SNG and CRI over India showed a much larger amplitude close to 200 ppb (Guha et al., 2018). The low amplitude at WLG was because of the high elevation of the continental mountain sites, where there were relatively fewer effects from local influences than the coastal/island sites (Yuan et al., 2019). Additionally, the seasonal amplitudes indicated different trends between the CR and TP. For the CR, the seasonal amplitude decreased at first and then increased over time, which was similar to the variation of the total regional events. But for the TP, the amplitude had a continuously increasing trend, with values of 15.1, 18.1, 21.4, 20.4, and 23.7 ppb in 1994-1997, 1998-2002, 2003-2007, 2008-2012, and 2013-2019, respectively. This revealed that the Tibetan Plateau was intensively affected by strong regional sources (e.g. grazing or emissions from India) over time.

3.6.2 Long-term trend

The fluctuating trend in atmospheric CH_4 during 1994-2019 at WLG (Fig. 12) was similar to the global trend reported by many studies (Bergamaschi et al., 2013; Rigby et al., 2017; Nisbet et al., 2019). In the 1990s, the CH_4 growth rates were very small or

even negative at WLG. Subsequently, a steady period with near-zero growth rates was found during 2002-2006. However, the atmospheric CH_4 increased significantly after 2007 (Fig. 12a). In 1997/1998, 2000/2001, 2007/2008, and 2011/2012, a large fluctuation in the growth rates was found and a strong growth appeared (Fig. 12b). The growth rates fluctuated evenly with both positive and negative values before 2009. However, almost all of the growth rates showed a positive value after 2009. Three developing stages (i.e. highlighted green, blue, and red blocks) could be seen from the 1990s to 2010s. The CH_4 mole fraction slightly decreased during 1998-2000 (green color), and then went through a relatively steady period during 2003-2006 (blue color), finally increased rapidly after 2007 (red color) (Fig. 12).

The annual growth rate was 5.1 ± 0.1 ppb yr^{-1} throughout 1994-2019 at WLG (Table 4). The periodic annual growth rates were 4.9 ± 0.1, 2.5 ± 0.2, 4.9 ± 0.1, 7.7 ± 0.1, and 5.5 ± 0.1 ppb yr^{-1} during 1994-1997, 1998-2002, 2003-2007, 2008-2012, and 2013-2019, respectively. Similar growth rates were found between the CR and the TP during 1994-2019 (Fig. S6). In 1994-1997 and 2003-2007, the growth rates in the TP were even larger than that in the CR (Table 4). These results indicated that there were also strong CH_4 sources from the TP. The previous study by Zhou et al. (2004) showed the annual increase in CH_4 by 4.5 ppb yr^{-1} in 1992-2001, which was close to our study in 1994-1997 and 1998-2002. Tohjima et al. (2002) found that the CH_4 levels at the Cape Ochi-ishi and Hateruma Island in1995-2000 respectively increased by 4.5 and 4.7 ppb yr^{-1}, which were also similar to that of WLG. Tsutsumi et al. (2006) analyzed the trend of hourly CH_4 data from 1998 to 2004 on the YON, which showed a similar increase (~3.0 ppb yr^{-1}) to WLG. The study at the GR and NW in Seoul, Korea, presented almost an identical trend of 2 ppb yr^{-1} between 2004 and 2013 (Ahmed et al., 2015), which was lower than that of WLG in similar period. In the early 1990s, the CH_4 growth rates at WLG were very low and similar to the global level. The level of •OH radicals might control the decrease or increase of CH_4 in the atmosphere during this period (Dlugokencky et al., 1998; Rigby et al., 2017; Turner et al., 2017). However, the

586 growth rates were high in 1998 (Fig. 12b), which may have been due to the high
587 temperatures and a large amount of biomass burning (Cunnold et al., 2002; Lelieveld
588 et al., 2004; Simmonds et al., 2005). The growth rate of CH_4 observed at the Ny-
589 Ålesund, Svalbard, increased from 0.3 ± 0.2 ppb yr^{-1} during 2000-2005 to 5.5 ± 0.2 ppb
590 yr^{-1} during 2005-2014, which had a similar variation but with a little lower growth rates
591 than that of WLG (Morimoto et al., 2017). The study suggested that the temporal pause
592 in 2000-2005 was ascribed to the reductions of CH_4 emissions from the microbial and
593 fossil fuel sectors, while the increase in 2005-2014 was due to an increase in microbial
594 release.

595 The constantly larger CH_4 growth rate after 2007 at WLG (Fig. 12) (Table 4) was
596 similar to the recent studies by Nisbet et al. (2016) and (2019), which showed that the
597 global CH_4 increased by 5.7 ± 1.2 ppb yr^{-1} in 2007-2014, and was much higher at 12.7
598 ± 0.5 ppb yr^{-1} in 2014, with 10.1 ± 0.7 ppb yr^{-1} in 2015, 7.0 ± 0.7 ppb yr^{-1} in 2016, and
599 7.7 ± 0.7 ppb yr^{-1} in 2017. The average growth rate in the Northern Hemisphere was
600 7.3 ± 1.3 ppb in 2007 and 8.1 ± 1.6 ppb in 2008 (Dlugokencky et al., 2009), which was
601 also similar to the observation at WLG (Table 4). After 2007, most sites in the Northern
602 Hemisphere had large CH_4 growth rates. Also, the average global growth rate was
603 similar to WLG at 7.1 ppb yr^{-1} in the most recent ten years (WMO, 2019). Fang et al.
604 (2013) showed that the annual growth rate of CH_4 was 9.4 ± 0.2 ppb yr^{-1} in 2009-2011
605 at WLG, which was a little higher than this study in 2008-2012. The adjacent stations
606 in China also revealed the high CH_4 growth rates of 8.0 ± 1.2 ppb yr^{-1} at Lin'an in 2009-
607 2011, 7.9 ± 0.9 ppb yr^{-1} at Longfengshan in 2009-2011, and 10 ± 0.1 ppb yr^{-1} at
608 Shangdianzi in 2009-2013 (Fang et al., 2013, 2016), which were all higher than the
609 similar periods of 2008-2012 or 2013-2019 at WLG (Table 4). The CH_4 measurements
610 in other countries, such as the Beromünster tall tower station, also showed a high
611 growth rate of 9.66 ppb yr^{-1} in 2012-2014 (Satar et al., 2016). The warm temperatures,
612 biomass burning, and the climatic anomalies (El Niño or La Niña), likely enhanced the
613 CH_4 emissions after 2007 (Dlugokencky et al., 2009). The anomalous years of

increasing or decreasing (e.g. 2007/2008) might have a significant influence on the overall CH_4 trend (Fig. 12). These frequent anomalies also appeared in most long-term observation stations, e.g. MLO in the USA (Dlugokencky et al., 2009) and Mount Zugspitze in Germany (Yuan et al., 2019), due to climatic forces, such as those exceptions during the El Niño oscillation, forest fires, volcanic eruptions, and extreme weather events (Keeling et al., 1995; Dlugokencky et al., 2009; Keenan et al., 2016; Nisbet et al., 2019).

Many studies have investigated the potential reasons for the anomalous increasing. The study by Satar et al. (2016) at Beromünster, Switzerland explained that the short-term spikes were possibly related to emissions from agricultural activities, while the longer-lasting peaks were because of air mass transport and mixing. The isotopic evidence suggested that the significant increase of biogenic emissions was the dominant factor for the CH_4 rise. This was especially true in the tropical wetlands that had strong rainfall anomalies, and agricultural sources such as rice paddies and ruminants were a cause while fossil fuel emissions were not the main cause (Nisbet et al., 2016). The study from thaw ponds at Arctic regions revealed that there had very weak correlation between the amount of CH_4 released from ponds and environmental factors, e.g. air temperature and atmospheric pressure (Burke et al., 2019). Sweeney et al. (2016) using 29-year of measurements on North Slope of Alaska (BRW) to investigate the sensitivity of CH_4 emissions to the temperature change, which revealed that despite the short-term temperature sensitivity increases CH_4 emissions, it would have little impact in the long term. However, up to now, the specific causes of such distinct variability through the years, including the spikes or near-zero CH_4 growth rates, have not yet been determined. It is well established that human activities were mainly responsible for the recent rapid CH_4 growth rates and anomalies. The analysis from EDGAR showed the CH_4 emission per sector in China (Fig. S7) (Crippa et al., 2019). During the observing period, the waste, oil, and natural gas combustion, and open burning continuously emitted large amounts of CH_4 into the air. After 2000, the CH_4 emissions from solid fuel increased

greatly in China. After 2003, the CH_4 emitted from rice cultivation also increased continuously (Fig. S7). The increased emissions from these sectors greatly contributed to the CH_4 increase at WLG, as well as the other regions in China. In addition, studies revealed that China's coal sector dominated the positive trend in recent years, which contributed to the highest proportion of anthropogenic CH_4 emissions (~33%) (Janssens-Maenhout et al., 2019; Miller et al., 2019). In 2010-2015, China's coal production increased (from 3400 to 4000 million metric tons), but CH_4 emissions from rice cultivation, agriculture practices, ruminants, waste, and oil/gas consumption only increased slightly if at all (EIA, USA). Therefore, the control measures of coal mining reduction or limiting natural gas and petroleum exploitation may play an important role in slowing down CH_4 emissions in China.

3.7 Case study for air mass transport

As described above, the northeast and southeast city regions might have acted as strong regional sources influencing the atmospheric CH_4 at WLG. Therefore, to analyze the effect of long-range transport of emissions from cities, the regionally representative data was further excluded by air mass transport, and the remaining regional records were denoted as 'TR'. First, the monthly cluster analysis was applied to hourly trajectories over 2005-2007, 2008-2012 and 2013-2017. Then, based on the cluster analysis, the clusters were divided into two groups, i.e. from city regions (red clusters in Fig. S8), and other (black clusters in Fig. S8). Finally, the regionally representative data were accordingly classified as two groups based on the cluster results (cities or other). The statistical results were presented in detail in Figure S8 and Table S3.

Consequently, the proportions of trajectories from cities were 40.3%, 32.5%, and 6.8% in 2005-2007, 2008-2012, and 2013-2017, respectively. About 22.8%, 35.6%, and 38.4% of the regional records were associated with air masses from city regions in 2005-2007, 2008-2012, and 2013-2017, respectively (Table 5). The average CH_4 values for the city region air masses (1863.0 ± 0.3 ppb) were higher than the other sectors

(1850.6 ± 0.2 ppb) (Fig. S9). The overall growth rates of the TR in the periods of 2005-2016 or 1994-2016 were similar to the original data series (Fig. S9). However, after excluding the CH_4 records for the air trajectory transports from city regions, the growth rates of the TR in 2008-2012 (10.1 ± 0.1 ppb yr^{-1}) and 2013-2017 (6.3 ± 0.1 ppb yr^{-1}) (Table 5) were higher than the original regional data series (i.e. 7.6 ± 0.2 and 5.7 ± 0.1 ppb yr^{-1}) (Table 4). These results suggested that there were possibly other strong CH_4 sources at WLG that were not from cities and the southwest region (Northern India) was the most likely contributor. The PSCF analysis also supported this result (Fig .7). At present, Northern India and Eastern China were the two largest sources of CH_4 at WLG (Fig. S10) (Crippa et al., 2019). Since the Tibetan Plateau was coincidently trapped in the middle of them, the atmospheric CH_4 at WLG was very likely dominated by long-range transport from these two regions. Although CH_4 emissions increased slowly during 1994-2002, a negative trend appeared (Fig. S10), significantly increased emissions were found in both southeast and southwest Asia after 2007. Chen et al. (2013) illustrated that the warming (0.2 °C per decade) in the Tibetan Plateau resulted in substantial emissions of CH_4 due to the thawed permafrost and melted glaciers. The rapid increase of CH_4 would probably make it difficult to meet the goals of carbon emission reduction in the future. This would be especially true with the scenario of quickly increasing CH_4 on the Qinghai-Tibetan Plateau due to the emissions from the two largest source regions of Northern India and Eastern China. The large growth rate of atmospheric CH_4 in the TP revealed that i) the atmospheric CH_4 at WLG was not predominantly influenced by eastern cities in recent years and ii) large amounts of CH_4 were transported from the Tibetan Plateau to WLG in recent years.

4 Conclusions

Three developing stages of atmospheric CH_4 at Mt. Waliguan from the 1990s to 2010s were found. The CH_4 mole fractions slightly decreased during 1998-2000, and then went through a relatively steady period during 2003-2006 and finally increased rapidly

after 2007. Although near-zero and even negative growth appeared in some periods, the overall CH_4 increased rapidly, especially in recent years. Although most areas around WLG had small contributions to the CH_4 emissions, two strong source regions were found from the northeast and southwest of the site. Northern India possibly has become a stronger contributor than city regions were in the past. The temporal patterns, the annual variations, the long-term trends, or the source distribution of CH_4 at WLG were all changed in recent years. We found that WLG was increasingly affected by local sources such as human activities. Additionally, the Tibetan Plateau was intensively affected by strong sources over time, which showed a larger growth rate than that of the city regions in some periods. The anomalous variation and unprecedented growth rate of the atmospheric CH_4 in this region revealed that it was urgent to control CH_4 emissions. Reducing the emissions from strong source sectors like coal mining, natural gas or solid fuel exploitation, and rice cultivation may play an important role on CH_4 emissions reduction in China.

Data availability. The gridded meteorological data (2004-2019) from NOAA-ARL was available at ftp://arlftp.arlhq.noaa.gov/pub/archives/gdas1/. The data from MLO, JFJ, MNM station was downloaded from World Data Centre for Greenhouse Gases (WDCGG) at https://gaw.kishou.go.jp/. The MBL data was available at ftp://aftp.cmdl.noaa.gov/data/trace_gases/CH_4/flask/surface/. The geographical distribution of annual emission data by Emissions Database for Global Atmospheric Research (EDGAR) was from website https://edgar.jrc.ec.europa.eu/overview.php?v=50_GHG.

Author contributions. SL, SF and ZF designed the research. SL performed the data processing with assistance of SF and MG. The station were monitored, maintained ML

and PL, and they collected, preprocessed, and provided the hourly observational dataset. SL and SF finished the manuscript with contributions from all the co-authors.

Competing interests. The authors declare that they have no conflict of interest.

Acknowledgments. This study was funded by the National Key Research and Development Program of China (2017YFC0209700). We also thanks to the staff who have contributed to the system installation and maintenance at the Waliguan in past decades.

References

Ahmed, E., Kim, K. H., Jeon, E. C., and Brown, R. J. C.: Long term trends of methane, non methane hydrocarbons, and carbon monoxide in urban atmosphere, Sci. Total Environ., 518, 595-604, 10.1016/j.scitotenv.2015.02.058, 2015.

Ashbaugh, L. L., Malm, W. C., and Sadeh, W. Z.: A residence time probability analysis of sulfur concentrations at grand-canyon-national-park, Atmos. Environ., 19, 1263-1270, 10.1016/0004-6981(85)90256-2, 1985.

Battle, M., Bender, M., Sowers, T., Tans, P. P., Butler, J. H., Elkins, J. W., Ellis, J. T., Conway, T., Zhang, N., Lang, P., and Clarke, A. D.: Atmospheric gas concentrations over the past century measured in air from firn at the south pole, Nature, 383, 231-235, 10.1038/383231a0, 1996.

Bergamaschi, P., Houweling, S., Segers, A., Krol, M., Frankenberg, C., Scheepmaker, R. A., Dlugokencky, E., Wofsy, S. C., Kort, E. A., Sweeney, C., Schuck, T., Brenninkmeijer, C., Chen, H., Beck, V., and Gerbig, C.: Atmospheric CH_4 in the first decade of the 21st century: Inverse modeling analysis using sciamachy satellite retrievals and NOAA surface measurements, J. Geophys. Res.-Atmos., 118, 7350-7369, 10.1002/jgrd.50480, 2013.

Blake, D. R., Mayer, E. W., Tyler, S. C., Makide, Y., Montague, D. C., and Rowland, F. S.: Global increase in atmospheric methane concentrations between 1978 and 1980, Geophys. Res. Lett., 9, 477-480, 10.1029/GL009i004p00477, 1982.

Bousquet, P., Ringeval, B., Pison, I., Dlugokencky, E. J., Brunke, E. G., Carouge, C., Chevallier, F., Fortems-Cheiney, A., Frankenberg, C., Hauglustaine, D. A., Krummel, P. B., Langenfelds, R. L., Ramonet, M., Schmidt, M., Steele, L. P., Szopa, S., Yver, C., Viovy, N., and Ciais, P.: Source attribution of the changes in atmospheric methane for 2006-2008, Atmos. Chem. Phys., 11, 3689-3700, 10.5194/acp-11-3689-2011, 2011.

Buchholz, R. R., Paton-Walsh, C., Griffith, D. W. T., Kubistin, D., Caldow, C., Fisher, J. A., Deutscher, N. M., Kettlewell, G., Riggenbach, M., Macatangay, R., Krummel,

765 P. B., and Langenfelds, R. L.: Source and meteorological influences on air quality
766 (CO, CH_4 & CO_2) at a Southern Hemisphere urban site, Atmos. Environ., 126, 274-
767 289, 10.1016/j.atmosenv.2015.11.041, 2016.
768 Burke, S. A., Wik, M., Lang, A., Contosta, A. R., Palace, M., Crill, M., and Varner, R.
769 K.: Long-term measurements of methane ebullition from thaw ponds, J. Geophys.
770 Res.-Biogeosci., 124, 2208-2221, 10.1029/2018jg004786, 2019.
771 Cai, Z. C., Tsuruta, H., and Minami, K.: Methane emission from rice fields in China:
772 Measurements and influencing factors, J. Geophys. Res.-Atmos., 105, 17231-17242,
773 10.1029/2000jd900014, 2000.
774 Carslaw, D. C., Beevers, S. D., Ropkins, K., and Bell, M. C.: Detecting and quantifying
775 aircraft and other on-airport contributions to ambient nitrogen oxides in the vicinity
776 of a large international airport, Atmos. Environ., 40, 5424-5434,
777 10.1016/j.atmosenv.2006.04.062, 2006.
778 Chen, H., Zhu, Q. A., Peng, C. H., Wu, N., Wang, Y. F., Fang, X. Q., Gao, Y. H., Zhu,
779 D., Yang, G., Tian, J. Q., Kang, X. M., Piao, S. L., Ouyang, H., Xiang, W. H., Luo,
780 Z. B., Jiang, H., Song, X. Z., Zhang, Y., Yu, G. R., Zhao, X. Q., Gong, P., Yao, T. D.,
781 and Wu, J. H.: The impacts of climate change and human activities on
782 biogeochemical cycles on the Qinghai-Tibetan Plateau, Glob. Change Biol., 19,
783 2940-2955, 10.1111/gcb.12277, 2013.
784 Crippa, M., Oreggioni, G., Guizzardi, D., Muntean, M., Schaaf, E., Lo Vullo, E.,
785 Solazzo, E., Monforti-Ferrario, F., Olivier, J.G.J., Vignati, E.: Fossil CO_2 and GHG
786 emissions of all world countries - 2019 Report, EUR 29849 EN, Publications Office
787 of the European Union, Luxembourg, ISBN 978-92-76-11100-9.
788 https://edgar.jrc.ec.europa.eu/overview.php?v=50_GHG, 2019.
789 Cunnold, D. M., Steele, L. P., Fraser, P. J., Simmonds, P. G., Prinn, R. G., Weiss, R. F.,
790 Porter, L. W., O'Doherty, S., Langenfelds, R. L., Krummel, P. B., Wang, H. J.,
791 Emmons, L., Tie, X. X., and Dlugokencky, E. J.: In situ measurements of
792 atmospheric methane at GAGE/AGAGE sites during 1985-2000 and resulting source

inferences, J. Geophys. Res.-Atmos., 107, 20, 10.1029/2001jd001226, 2002.

Diederich, A.: Generalized additive models. An introduction with R, J. Math. Psychol., 51, 339-339, 2007.

Dlugokencky, E. J., Steele, L. P., Lang, P. M., and Masarie, K. A.: The growth-rate and distribution of atmospheric methane, J. Geophys. Res.-Atmos., 99, 17021-17043, 10.1029/94jd01245, 1994.

Dlugokencky, E. J., Steele, L. P., Lang, P. M., and Masarie, K. A.: Atmospheric methane at Mauna-Loa and Barrow observatories - presentation and analysis of in-situ measurements, J. Geophys. Res.-Atmos., 100, 23103-23113, 10.1029/95jd02460, 1995.

Dlugokencky, E. J., Masarie, K. A., Lang, P. M., and Tans, P. P.: Continuing decline in the growth rate of the atmospheric methane burden, Nature, 393, 447-450, 10.1038/30934, 1998.

Dlugokencky, E. J., Bruhwiler, L., White, J. W. C., Emmons, L. K., Novelli, P. C., Montzka, S. A., Masarie, K. A., Lang, P. M., Crotwell, A. M., Miller, J. B., and Gatti, L. V.: Observational constraints on recent increases in the atmospheric CH_4 burden, Geophys. Res. Lett., 36, 5, 10.1029/2009gl039780, 2009.

Dlugokencky, E.J., Crotwell, A.M., Lang, P.M., and Mund, J.W.: Atmospheric Methane Dry Air Mole Fractions from quasi-continuous measurements at Barrow, Alaska and Mauna Loa, Hawaii, 1986-2018, Version: 2019-03-04, Path: ftp://aftp.cmdl.noaa.gov/data/trace_gases/CH_4/in-situ/surface/, 2019a.

Dlugokencky, E.J., Lang, P.M., Crotwell, A.M., Thoning, K.W., and M.J. Crotwell.: Atmospheric Methane Dry Air Mole Fractions from the NOAA ESRL Carbon Cycle Cooperative Global Air Sampling Network. Data Path: ftp://aftp.cmdl.noaa.gov/data/trace_gases/CH_4/flask/surface/, 2019b.

Draxier, R. R., and Hess, G. D.: An overview of the hysplit_4 modelling system for trajectories, dispersion and deposition, Aust. Meteorol. Mag., 47, 295-308, 1998.

Etheridge, D. M., Steele, L. P., Francey, R. J., and Langenfelds, R. L.: Atmospheric

821 methane between 1000 AD and present: Evidence of anthropogenic emissions and
822 climatic variability, J. Geophys. Res.-Atmos., 103, 15979-15993,
823 10.1029/98jd00923, 1998.
824 Etminan, M., Myhre, G., Highwood, E. J., and Shine, K. P.: Radiative forcing of carbon
825 dioxide, methane, and nitrous oxide: A significant revision of the methane radiative
826 forcing, Geophys. Res. Lett., 43, 12614-12623, 10.1002/2016gl071930, 2016.
827 Fang, S. X., Zhou, L. X., Masarie, K. A., Xu, L., and Rella, C. W.: Study of atmospheric
828 CH_4 mole fractions at three WMO/GAW stations in China, J. Geophys. Res.-Atmos.,
829 118, 4874-4886, 10.1002/jgrd.50284, 2013.
830 Fang, S. X., Tans, P. P., Dong, F., Zhou, H. G., and Luan, T.: Characteristics of
831 atmospheric CO_2 and CH_4 at the Shangdianzi regional background station in China,
832 Atmos. Environ., 131, 1-8, 10.1016/j.atmosenv.2016.01.044, 2016.
833 Fu, X. W., Feng, X., Liang, P., Zhang, H., Ji, J., and Liu, P.: Temporal trend and sources
834 of speciated atmospheric mercury at Waliguan GAW station, northwestern China,
835 Atmos. Chem. Phys., 12, 1951-1964, 10.5194/acp-12-1951-2012, 2012.
836 Galloway, J. N.: Atmospheric acidification - projections for the future, Ambio, 18, 161-
837 166, 1989.
838 Guha, T., Tiwari, Y. K., Valsala, V., Lin, X., Ramonet, M., Mahajan, A., Datye, A., and
839 Kumar, K. R.: What controls the atmospheric methane seasonal variability over
840 India?, Atmos. Environ., 175, 83-91, 10.1016/j.atmosenv.2017.11.042, 2018.
841 Hausmann, P., Sussmann, R., and Smale, D.: Contribution of oil and natural gas
842 production to renewed increase in atmospheric methane (2007-2014): Top-down
843 estimate from ethane and methane column observations, Atmos. Chem. Phys., 16,
844 3227-3244, 10.5194/acp-16-3227-2016, 2016.
845 IPCC, Climate Change 2014: Synthesis Report. Contribution of Working Groups I, II
846 and III to the Fifth Assessment Report of the Intergovernmental Panel on Climate
847 Change [Core Writing Team, R.K. Pachauri and L.A. Meyer (eds.)]. IPCC, Geneva,
848 Switzerland, 151 pp, 2014.

Janssens-Maenhout, G., Crippa, M., Guizzardi, D., Muntean, M., Schaaf, E., Dentener, F., Bergamaschi, P., Pagliari, V., Olivier, J. G. J., Peters, J., van Aardenne, J. A., Monni, S., Doering, U., Petrescu, A. M. R., Solazzo, E., and Oreggioni, G. D.: Edgar v4.3.2 global atlas of the three major greenhouse gas emissions for the period 1970-2012, Earth Syst. Sci. Data, 11, 959-1002, 10.5194/essd-11-959-2019, 2019.

Keeling, C. D., Bacastow, R. B., Bainbridge, A. E., Ekdahl, C. A., Guenther, P. R., Waterman, L. S., and Chin, J. F. S.: Atmospheric carbon-dioxide variations at Mauna-Loa observatory, Hawaii, Tellus, 28, 538-551, 1976.

Keeling, C. D., Whorf, T. P., Wahlen, M., and Vanderplicht, J.: Interannual extremes in the rate of rise of atmospheric carbon-dioxide since 1980, Nature, 375, 666-670, 10.1038/375666a0, 1995.

Keenan, T. F., Prentice, I. C., Canadell, J. G., Williams, C. A., Wang, H., Raupach, M., and Collatz, G. J.: Recent pause in the growth rate of atmospheric CO_2 due to enhanced terrestrial carbon uptake, Nat. Commun., 7, 9, 10.1038/ncomms13428, 2016.

Kim, H. S., Chung, Y. S., Tans, P. P., and Dlugokencky, E. J.: Decadal trends of atmospheric methane in East Asia from 1991 to 2013, Air Qual. Atmos. Health, 8, 293-298, 10.1007/s11869-015-0331-x, 2015.

Lelieveld, J., Dentener, F. J., Peters, W., and Krol, M. C.: On the role of hydroxyl radicals in the self-cleansing capacity of the troposphere, Atmos. Chem. Phys., 4, 2337-2344, 10.5194/acp-4-2337-2004, 2004.

Lin, M. Y., Horowitz, L. W., Oltmans, S. J., Fiore, A. M., and Fan, S. M.: Tropospheric ozone trends at Mauna Loa observatory tied to decadal climate variability, Nat. Geosci., 7, 136-143, 10.1038/ngeo2066, 2014.

Liu, S., Fang, S. X., Liang, M., Ma, Q. L., and Feng, Z. Z.: Study on CO data filtering approaches based on observations at two background stations in China, Sci. Total Environ., 691, 675-684, 10.1016/j.scitotenv.2019.07.162, 2019.

Logan, J. A., Prather, M. J., Wofsy, S. C., and McElroy, M. B.: Tropospheric chemistry

877 - a global perspective, J. Geophys. Res.-Oceans, 86, 7210-7254,
878 10.1029/JC086iC08p07210, 1981.
879 Loov, J. M. B., Henne, S., Legreid, G., Staehelin, J., Reimann, S., Prevot, A. S. H.,
880 Steinbacher, M., and Vollmer, M. K.: Estimation of background concentrations of
881 trace gases at the Swiss Alpine site Jungfraujoch (3580 m asl), J. Geophys. Res.-
882 Atmos., 113, 17, 10.1029/2007jd009751, 2008.
883 Ma, J. Z., Tang, J., Zhou, X. J., and Zhang, X. S.: Estimates of the chemical budget for
884 ozone at Waliguan observatory, J. Atmos. Chem., 41, 21-48,
885 10.1023/a:1013892308983, 2002.
886 Matsueda, H. et al., Methane standard gases for atmospheric measurements at the MRI
887 and JMA and intercomparison experiments, Pap. Meteor. Geophys., 54, 91-109,
888 2004.
889 Miller, S. M., Michalak, A. M., Detmers, R. G., Hasekamp, O. P., Bruhwiler, L. M. P.,
890 and Schwietzke, S.: China's coal mine methane regulations have not curbed growing
891 emissions, Nat. Commun., 10, 8, 10.1038/s41467-018-07891-7, 2019.
892 Morimoto, S., Fujita, R., Aoki, S., Goto, D., and Nakazawa, T.: Long-term variations
893 of the mole fraction and carbon isotope ratio of atmospheric methane observed at
894 Ny-angstrom lesund, svalbard from 1996 to 2013, Tellus Ser. B-Chem. Phys.
895 Meteorol., 69, 7, 10.1080/16000889.2017.1380497, 2017.
896 Nisbet, E. G., Dlugokencky, E. J., and Bousquet, P.: Methane on the rise-again, Science,
897 343, 493-495, 10.1126/science.1247828, 2014.
898 Nisbet, E. G., Dlugokencky, E. J., Manning, M. R., Lowry, D., Fisher, R. E., France, J.
899 L., Michel, S. E., Miller, J. B., White, J. W. C., Vaughn, B., Bousquet, P., Pyle, J. A.,
900 Warwick, N. J., Cain, M., Brownlow, R., Zazzeri, G., Lanoisellé, M., Manning, A.
901 C., Gloor, E., Worthy, D. E. J., Brunke, E.-G., Labuschagne, C., Wolff, E. W., and
902 Ganesan, A. L.: Rising atmospheric methane: 2007-2014 growth and isotopic shift,
903 Global Biogeochem. Cy., 30, 1356-1370, 10.1002/2016gb005406, 2016.
904 Nisbet, E. G., Manning, M. R., Dlugokencky, E. J., Fisher, R. E., Lowry, D., Michel, S.

E., Myhre, C. L., Platt, S. M., Allen, G., Bousquet, P., Brownlow, R., Cain, M., France, J. L., Hermansen, O., Hossaini, R., Jones, A. E., Levin, I., Manning, A. C., Myhre, G., Pyle, J. A., Vaughn, B. H., Warwick, N. J., and White, J. W. C.: Very strong atmospheric methane growth in the 4 years 2014-2017: Implications for the paris agreement, Global Biogeochem. Cy., 33, 318-342, 10.1029/2018gb006009, 2019.

Niwa, Y., Tsuboi, K., Matsueda, H., Sawa, Y., Machida, T., Nakamura, M., Kawasato, T., Saito, K., Takatsuji, S., Tsuji, K., Nishi, H., Dehara, K., Baba, Y., Kuboike, D., Iwatsubo, S., Ohmori, H., and Hanamiya, Y.: Seasonal variations of CO_2, CH_4, N_2O and CO in the mid-troposphere over the western North Pacific observed using a C-130H cargo aircraft, J. Meteorol. Soc. Jpn., 92, 55-70, 10.2151/jmsj.2014-104, 2014.

Pearman, G. I., and Beardsmore, D. J.: Atmospheric carbon-dioxide measurements in the Australian region - 10 years of aircraft data, Tellus Ser. B-Chem. Phys. Meteorol., 36, 1-24, 10.1111/j.1600-0889.1984.tb00047.x, 1984.

Polissar, A. V., Hopke, P. K., Paatero, P., Kaufmann, Y. J., Hall, D. K., Bodhaine, B. A., Dutton, E. G., and Harris, J. M.: The aerosol at barrow, alaska: Long-term trends and source locations, Atmos. Environ., 33, 2441-2458, 10.1016/s1352-2310(98)00423-3, 1999.

Popa, M. E., Gloor, M., Manning, A. C., Jordan, A., Schultz, U., Haensel, F., Seifert, T., and Heimann, M.: Measurements of greenhouse gases and related tracers at Bialystok tall tower station in Poland, Atmos. Meas. Tech., 3, 407-427, 10.5194/amt-3-407-2010, 2010.

Press, W. H., Flannery, B. P., Teukolsky, S. A., and Vetterling, W. T.: Numerical recipes in C: The art of scientific programming, Section, 10, 408-412, 1992.

Rasmussen, R. A., and Khalil, M. A. K.: Atmospheric methane in the recent and ancient atmospheres - concentrations, trends, and interhemispheric gradient, J. Geophys. Res.-Atmos., 89, 1599-1605, 10.1029/JD089iD07p11599, 1984.

R Core Team.: R: a language and environment for statistical computing. R Foundation

for Statistical Computing, Vienna, Austria, URL: http://www.R-project.org/, 2020.

Rigby, M., Montzka, S. A., Prinn, R. G., White, J. W. C., Young, D., O'Doherty, S., Lunt, M. F., Ganesan, A. L., Manning, A. J., Simmonds, P. G., Salameh, P. K., Harth, C. M., Muhle, J., Weiss, R. F., Fraser, P. J., Steele, L. P., Krummel, P. B., McCulloch, A., and Park, S.: Role of atmospheric oxidation in recent methane growth, Proc. Natl. Acad. Sci. U. S. A., 114, 5373-5377, 10.1073/pnas.1616426114, 2017.

Rousseau, D. D., Duzer, D., Etienne, J. L., Cambon, G., Jolly, D., Ferrier, J., and Schevin, P.: Pollen record of rapidly changing air trajectories to the North Pole, J. Geophys. Res.-Atmos., 109, 10.1029/2003jd003985, 2004.

Rubino, M., Etheridge, D. M., Thornton, D. P., Howden, R., Allison, C. E., Francey, R. J., Langenfelds, R. L., Steele, L. P., Trudinger, C. M., Spencer, D. A., Curran, M. A. J., van Ommen, T. D., and Smith, A. M.: Revised records of atmospheric trace gases CO_2, CH_4, N_2O, and delta C-13-CO_2 over the last 2000 years from Law Dome, Antarctica, Earth Syst. Sci. Data, 11, 473-492, 10.5194/essd-11-473-2019, 2019.

Satar, E., Berhanu, T. A., Brunner, D., Henne, S., and Leuenberger, M.: Continuous CO_2/CH_4/CO measurements (2012-2014) at Beromunster tall tower station in Switzerland, Biogeosciences, 13, 2623-2635, 10.5194/bg-13-2623-2016, 2016.

Saunois, M., Bousquet, P., Poulter, B., Peregon, A., Ciais, P., Canadell, J. G., Dlugokencky, E. J., Etiope, G., Bastviken, D., Houweling, S., Janssens-Maenhout, G., Tubiello, F. N., Castaldi, S., Jackson, R. B., Alexe, M., Arora, V. K., Beerling, D. J., Bergamaschi, P., Blake, D. R., Brailsford, G., Brovkin, V., Bruhwiler, L., Crevoisier, C., Crill, P., Covey, K., Curry, C., Frankenberg, C., Gedney, N., Hoglund-Isaksson, L., Ishizawa, M., Ito, A., Joos, F., Kim, H. S., Kleinen, T., Krummel, P., Lamarque, J. F., Langenfelds, R., Locatelli, R., Machida, T., Maksyutov, S., McDonald, K. C., Marshall, J., Melton, J. R., Morino, I., Naik, V., O'Doherty, S., Parmentier, F. J. W., Patra, P. K., Peng, C. H., Peng, S. S., Peters, G. P., Pison, I., Prigent, C., Prinn, R., Ramonet, M., Riley, W. J., Saito, M., Santini, M., Schroeder, R., Simpson, I. J., Spahni, R., Steele, P., Takizawa, A., Thornton, B. F., Tian, H. Q.,

961 Tohjima, Y., Viovy, N., Voulgarakis, A., van Weele, M., van der Werf, G. R., Weiss,
962 R., Wiedinmyer, C., Wilton, D. J., Wiltshire, A., Worthy, D., Wunch, D., Xu, X. Y.,
963 Yoshida, Y., Zhang, B., Zhang, Z., and Zhu, Q.: The global methane budget 2000-
964 2012, Earth Syst. Sci. Data, 8, 697-751, 10.5194/essd-8-697-2016, 2016.
965 Saunois, M., Stavert, A.R., Poulter, B. et al.: The Global Methane Budget 2000-2017,
966 Earth Syst. Sci. Data, https://doi.org/10.5194/essd-2019-128, 2019.
967 Schaefer, H., Fletcher, S. E. M., Veidt, C., Lassey, K. R., Brailsford, G. W., Bromley, T.
968 M., Dlugokencky, E. J., Michel, S. E., Miller, J. B., Levin, I., Lowe, D. C., Martin,
969 R. J., Vaughn, B. H., and White, J. W. C.: A 21st-century shift from fossil-fuel to
970 biogenic methane emissions indicated by (CH_4)-C-13, Science, 352, 80-84,
971 10.1126/science.aad2705, 2016.
972 Simmonds, P. G., Manning, A. J., Derwent, R. G., Ciais, P., Ramonet, M., Kazan, V.,
973 and Ryall, D.: A burning question. Can recent growth rate anomalies in the
974 greenhouse gases be attributed to large-scale biomass burning events?, Atmos.
975 Environ., 39, 2513-2517, 10.1016/j.atmosenv.2005.02.018, 2005.
976 Streets, D. G., and Waldhoff, S. T.: Present and future emissions of air pollutants in
977 China: SO_2, NO_x, and CO, Atmos. Environ., 34, 363-374, 10.1016/s1352-
978 2310(99)00167-3, 2000.
979 Sweeney, C., Dlugokencky, E., Miller, C. E., Wofsy, S., Karion, A., Dinardo, S., Chang,
980 R. Y. W., Miller, J. B., Bruhwiler, L., Crotwell, A. M., Newberger, T., McKain, K.,
981 Stone, R. S., Wolter, S. E., Lang, P. E., and Tans, P.: No significant increase in long-
982 term CH_4 emissions on north slope of Alaska despite significant increase in air
983 temperature, Geophys. Res. Lett., 43, 6604-6611, 10.1002/2016gl069292, 2016.
984 Tang, J., Wen, Y. P., and Zhou, L. X.:, Observational study of black carbon aerosol in
985 western China, J. Appl. Meteor. Sci., 10, 160-170, 1999.
986 Thompson, R. L., Manning, A. C., Gloor, E., Schultz, U., Seifert, T., Hansel, F., Jordan,
987 A., and Heimann, M.: In-situ measurements of oxygen, carbon monoxide and
988 greenhouse gases from Ochsenkopf tall tower in Germany, Atmos. Meas. Tech., 2,

573-591, 10.5194/amt-2-573-2009, 2009.

Tohjima, Y., Machida, T., Utiyama, M., Katsumoto, M., Fujinuma, Y., and Maksyutov, S.: Analysis and presentation of in situ atmospheric methane measurements from Cape Ochi-ishi and Hateruma island, J. Geophys. Res.-Atmos., 107, 11, 10.1029/2001jd001003, 2002.

Tohjima, Y., Kubo, M., Minejima, C., Mukai, H., Tanimoto, H., Ganshin, A., Maksyutov, S., Katsumata, K., Machida, T., and Kita, K.: Temporal changes in the emissions of CH_4 and CO from China estimated from CH_4/CO_2 and CO/CO_2 correlations observed at Hateruma island, Atmos. Chem. Phys., 14, 1663-1677, 10.5194/acp-14-1663-2014, 2014.

Thoning, K. W., Tans, P. P., and Komhyr, W. D.: Atmospheric carbon dioxide at Mauna Loa observatory: 2. Analysis of the NOAA GMCC data, 1974-1985, J. Geophys. Res.-Atmos., 94, 8549-8565, 10.1029/JD094iD06p08549, 1989.

Tsutsumi, Y., Mori, K., Ikegami, M., Tashiro, T., and Tsuboi, K.: Long-term trends of greenhouse gases in regional and background events observed during 1998-2004 at Yonagunijima located to the east of the Asian continent, Atmos. Environ., 40, 5868-5879, 10.1016/j.atmosenv.2006.04.036, 2006.

Turner, A. J., Frankenbergb, C., Wennberg, P. O., and Jacob, D. J.: Ambiguity in the causes for decadal trends in atmospheric methane and hydroxyl, Proc. Natl. Acad. Sci. U. S. A., 114, 5367-5372, 10.1073/pnas.1616020114, 2017.

Uria-Tellaetxe, I., and Carslaw, D. C.: Conditional bivariate probability function for source identification, Environ. Modell. Softw., 59, 1-9, 10.1016/j.envsoft.2014.05.002, 2014.

US EIA (US Energy Information Administration): International energy statistics, available at https://www.eia.gov/ beta/international/data/browser/.

Vaghjiani, G. L., and Ravishankara, A. R.: New measurement of the rate coefficient for the reaction of OH with methane, Nature, 350, 406-409, 10.1038/350406a0, 1991.

Wada, A., Sawa, Y., Matsueda, H., Taguchi, S., Murayama, S., Okubo, S., and Tsutsumi,

Y.: Influence of continental air mass transport on atmospheric CO_2 in the western North Pacific, J. Geophys. Res.-Atmos., 112, 12, 10.1029/2006jd007552, 2007.

Wada, A., Matsueda, H., Sawa, Y., Tsuboi, K., and Okubo, S.: Seasonal variation of enhancement ratios of trace gases observed over 10 years in the western North Pacific, Atmos. Environ., 45, 2129-2137, 10.1016/j.atmosenv.2011.01.043, 2011.

Wang, D. Q., Chen, Z. L., and Xu, S. Y.: Methane emission from Yangtze estuarine wetland, china, J. Geophys. Res.-Biogeosci., 114, 11, 10.1029/2008jg000857, 2009.

Wang, T., Cheung, T. F., Li, Y. S., Yu, X. M., and Blake, D. R.: Emission characteristics of CO, NO_X, SO_2 and indications of biomass burning observed at a rural site in eastern China, J. Geophys. Res.-Atmos., 107, 10, 10.1029/2001jd000724, 2002.

Weber, T., Wiseman, N. A., and Kock, A.: Global ocean methane emissions dominated by shallow coastal waters, Nat. Commun., 10, 10, 10.1038/s41467-019-12541-7, 2019.

Wilson, M. C., and Smith, A. T.: The pika and the watershed: The impact of small mammal poisoning on the ecohydrology of the Qinghai-Tibetan Plateau, Ambio, 44, 16-22, 10.1007/s13280-014-0568-x, 2015.

WMO, WMO Greenhouse Gas Bulletin No.15, 2019.

WMO, WMO World Data Centre for Greenhouse Gases (WDCGG) Data Summary: Greenhouse Gases and Other Atmospheric Gases, No. 43. Japan Meteorological Agency, avaliablle at https://gaw.kishou.go.jp/static/publications/summary/sum43/sum43.pdf, 2020.

Wolf, J., Asrar, G. R., and West, T. O.: Revised methane emissions factors and spatially distributed annual carbon fluxes for global livestock, Carbon Balanc. Manag., 12, 24, 10.1186/s13021-017-0084-y, 2017.

Xiong, X., Houweling, S., Wei, J., Maddy, E., Sun, F., and Barnet, C.: Methane plume over South Asia during the monsoon season: Satellite observation and model simulation, Atmos. Chem. Phys., 9, 783-794, 10.5194/acp-9-783-2009, 2009.

Yuan, Y., Ries, L., Petermeier, H., Trickl, T., Leuchner, M., Couret, C., Sohmer, R.,

1045 Meinhardt, F., and Menzel, A.: On the diurnal, weekly, and seasonal cycles and
1046 annual trends in atmospheric CO_2 at Mount Zugspitze, Germany, during 1981-2016,
1047 Atmos. Chem. Phys., 19, 999-1012, 10.5194/acp-19-999-2019, 2019.
1048 Zellweger, C., Emmenegger, L., Firdaus, M., Hatakka, J., Heimann, M., Kozlova, E.,
1049 Spain, T. G., Steinbacher, M., van der Schoot, M. V., and Buchmann, B.: Assessment
1050 of recent advances in measurement techniques for atmospheric carbon dioxide and
1051 methane observations, Atmos. Meas. Tech., 9, 4737-4757, 10.5194/amt-9-4737-
1052 2016, 2016.
1053 Zhang, F., Zhou, L. X., Novelli, P. C., Worthy, D. E. J., Zellweger, C., Klausen, J., Ernst,
1054 M., Steinbacher, M., Cai, Y. X., Xu, L., Fang, S. X., and Yao, B.: Evaluation of in
1055 situ measurements of atmospheric carbon monoxide at Mount Waliguan, china,
1056 Atmos. Chem. Phys., 11, 5195-5206, 10.5194/acp-11-5195-2011, 2011.
1057 Zhang, F., Zhou, L., and Xu, L.: Temporal variation of atmospheric CH_4 and the
1058 potential source regions at Waliguan, China, Sci. China Earth Sci., 56, 727-736,
1059 10.1007/s11430-012-4577-y, 2013.
1060 Zhou, L., Worthy, D. E. J., Lang, P. M., Ernst, M. K., Zhang, X. C., Wen, Y. P., and Li,
1061 J. L.: Ten years of atmospheric methane observations at a high elevation site in
1062 western China, Atmos. Environ., 38, 7041-7054, 10.1016/j.atmosenv.2004.02.072,
1063 2004.
1064 Zhou, L. X., Conway, T. J., White, J. W. C., Mukai, H., Zhang, X. C., Wen, Y. P., Li, J.
1065 L., and MacClune, K.: Long-term record of atmospheric CO_2 and stable isotopic
1066 ratios at Waliguan observatory: Background features and possible drivers, 1991-
1067 2002, Global Biogeochem. Cy., 19, 9, 10.1029/2004gb002430, 2005.
1068 Zhou, L. X., Tang, J., Wen, Y. P., Li, J. L., Yan, P., and Zhang, X. C.: The impact of
1069 local winds and long-range transport on the continuous carbon dioxide record at
1070 Mount Waliguan, China, Tellus Ser. B-Chem. Phys. Meteorol., 55, 145-158,
1071 10.1034/j.1600-0889.2003.00064.x, 2003.
1072 Zou, J. W., Huang, Y., Jiang, J. Y., Zheng, X. H., and Sass, R. L.: A 3-year field

measurement of methane and nitrous oxide emissions from rice paddies in China: Effects of water regime, crop residue, and fertilizer application, Global Biogeochem. Cy., 19, 9, 10.1029/2004gb002401, 2005.

1076 **Table 1.** The statistics of the filtered CH_4 data series over different periods during 1994-2019 at

1077 WLG station.

Year	Regionally representative			Locally influenced		
	Hours	Percentage (%)	Mean (ppb)	Hours	Percentage (%)	Mean (ppb)
1994-1997	16122	71.3	1801.7 ± 0.5	6481	28.7	1806.2 ± 0.3
1998-2002	26347	83.2	1832.6 ± 0.7	5336	16.8	1837.7 ± 0.3
2003-2007	28181	69.4	1832.3± 0.3	12443	30.6	1839.2 ± 0.2
2008-2012	19627	63.5	1856.2 ± 0.4	11287	36.5	1865.2 ± 0.3
2013-2019	21683	44.2	1906.8 ± 0.3	27329	55.8	1920.4 ± 0.4
1994-2019	111960	64.0	1865.8 ± 0.4	62876	36.0	1868.2 ± 0.3

1078

1079 **Table 2.** Yearly average CH_4 mole fractions at WLG station.

Year	Mean (ppb)	year	Mean (ppb)
1994	1799.0 ± 0.4	2007	1837.2 ± 0.5
1995	1803.6 ± 0.1	2008	1854.8 ± 0.1
1996	1808.8 ± 0.2	2009	1847.2 ± 0.1
1997	1811.5 ± 0.2	2010	1856.6 ± 0.2
1998	1826.8 ± 0.1	2011	1867.4 ± 0.1
1999	1819.7 ± 0.1	2012	1879.6 ± 0.2
2000	1819.7 ± 0.2	2013	1895.7 ± 0.4
2001	1847.3 ± 0.4	2014	1890.2 ± 0.2
2002	1833.7 ± 0.2	2015	1913.0 ± 0.4
2003	1840.8 ± 0.2	2016	1914.4 ± 0.2
2004	1836.1 ± 0.2	2017	1911.6 ± 0.1
2005	1836.7 ± 0.1	2018	1925.6 ± 0.3
2006	1834.7 ± 0.2	2019	1932.0 ± 0.1

1080

Table 3. The statistics for the cluster analysis result for hourly CH_4 data from 2004-2019 at WLG station. The clusters from urban areas are highlighted in bold.

	Cluster	Number	Average CH_4 mole fraction
Spring	1	2601	1867.0 ± 1.5
	2	**1836**	**1882.7 ± 2.0**
	3	2678	1881.8 ± 1.4
Summer	1	1250	1898.5 ± 2.1
	2	1694	1899.4 ± 1.6
	3	**2310**	**1889.5 ± 1.6**
Autumn	1	1188	1913.1 ± 2.2
	2	2487	1880.2 ± 1.5
	3	2217	1887.7 ± 1.6
Winter	1	2218	1882.9 ± 1.7
	2	**791**	**1920.6 ± 2.9**
	3	4482	1877.2 ± 1.0

Table 4. Annual growth rates of atmospheric CH_4 in the City Regions (CR), the Tibetan Plateau (TP), and total regional records from 1994 to 2019 at WLG station.

	1994-1997	1998-2002	2003-2007	2008-2012	2013-2019	1994-2019
CR	3.0 ± 0.1	3.6 ± 0.2	5.3 ± 0.2	7.0 ± 0.2	6.2 ± 0.1	5.2 ± 0.1
TP	3.4 ± 0.1	3.0 ± 0.2	6.7 ± 0.2	5.7 ± 0.2	5.7 ± 0.1	5.1 ± 0.1
Total	4.9 ± 0.1	2.5 ± 0.2	4.9 ± 0.1	7.7 ± 0.1	5.5 ± 0.1	5.1 ± 0.1

Table 5. The statistics of CH_4 data without air mass transport from city regions (TR) over different periods during 2005-2016 at WLG station.

	Transport regions	Hours	Percentage (%)	Average (ppb)	Updated growth rate (ppb yr-1)
2005-2007	TR	6922	77.2	1824.9 ± 0.2	2.7 ± 0.2
	City	2041	22.8	1835.9 ± 0.5	-
2008-2012	TR	7060	64.4	1853.7 ± 0.2	10.1 ± 0.1
	City	4254	35.6	1861.0 ± 0.3	-
2013-2016	TR	4152	61.6	1888.2 ± 0.3	6.3 ± 0.1
	City	2591	38.4	1888.5 ± 0.5	-
2005-2016	TR	18134	67.1	1850.6 ± 0.2	7.0 ± 0.1
	City	8886	32.9	1863.2 ± 0.3	-

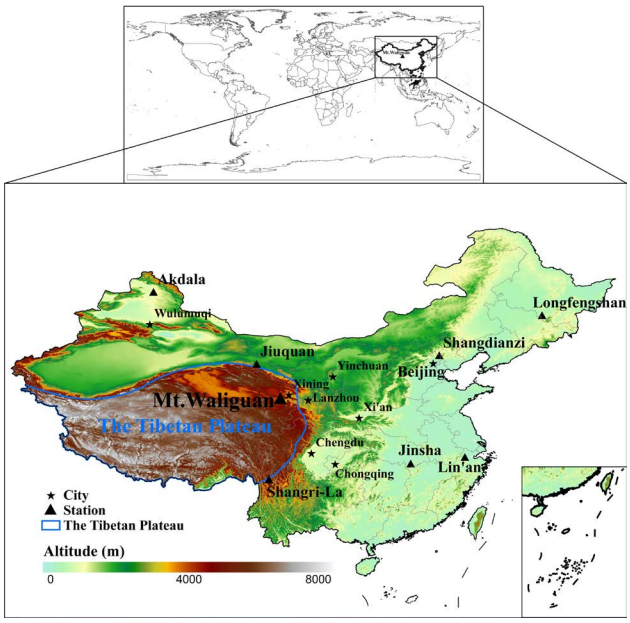

Figure 1. The location of Mt. Waliguan WMO/GAW global station as well as the other regional stations in China. The gradient color indicates altitude. The digital elevation model (DEM) was downloaded from Geospatial Data Cloud site, Computer Network Information Center, Chinese Academy of Sciences (http://www.gscloud.cn), and then processed by ArcGis software. The China map was derived from © National basic Geomatics Center of China (http://www.ngcc.cn/ngcc/). The world map was obtained from © OpenStreetMap (https://www.openstreetmap.org/).

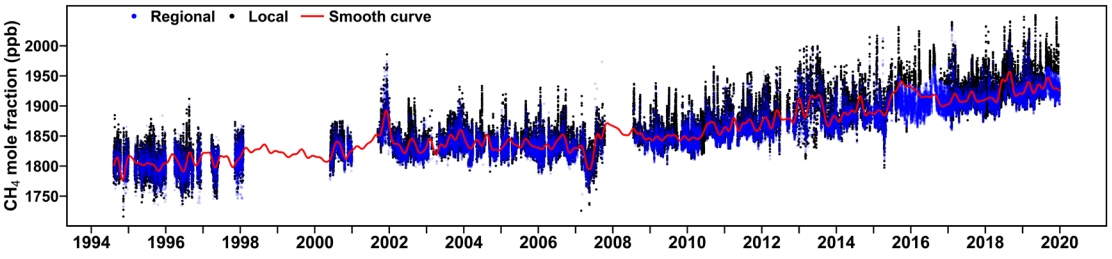

Figure 2. The filtered hourly CH_4 data series from 1994 to 2019 at WLG station. The transparent blue points are regionally representative data. The black points are locally influenced data. The red lines are smooth values of the regional data obtained by the curve-fitting routine of Thoning et al. (1989).

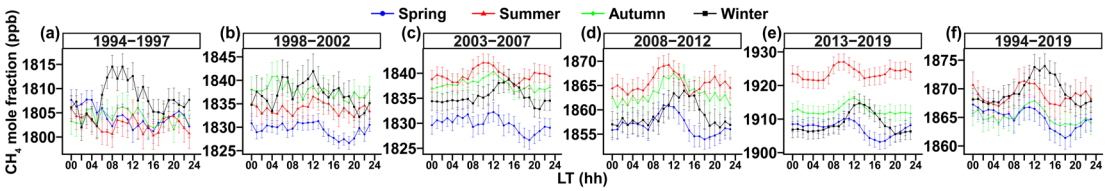

Figure 3. Diurnal CH_4 cycles in different periods from 1994 to 2019 at WLG station. The lines with different colors represent various seasons. Error bars indicate the 95% confidence intervals.

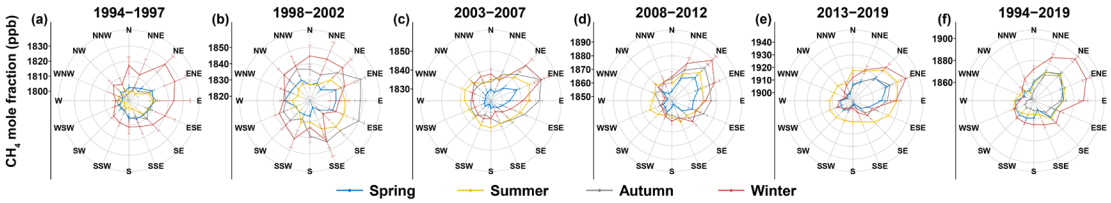

1105

1106 **Figure 4.** The wind-rose distribution of the average CH_4 mole fractions from 16 horizontal wind

1107 directions over different periods during 1994-2019 at WLG station. The different colors represent

1108 the CH_4 data in different seasons. Error bars in all directions indicate 95% confidence intervals.

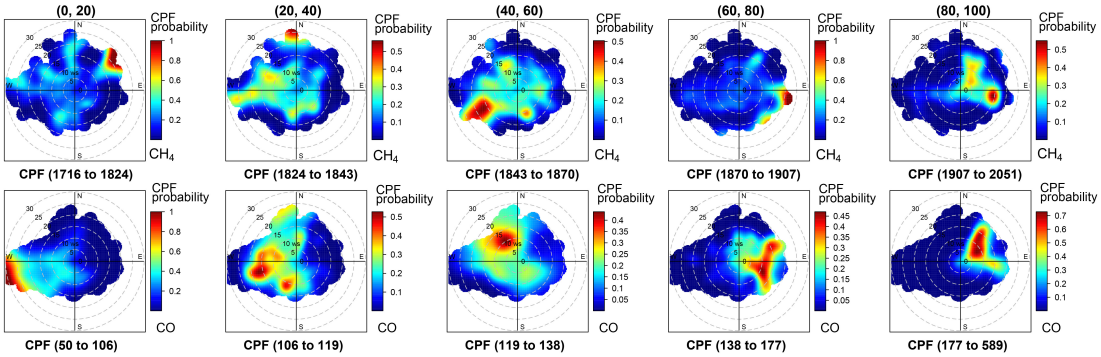

Figure 5. The polar plot of the distribution of the CH_4 and CO concentration probabilities in different percentile ranges at WLG station. The analysis was based on conditional probability functions (CPF) by Ashbaugh et al. (1985). The top plots show the analysis of CH_4 from 1994 to 2019. The bottom plots show the CO measurements in 2004-2019. 'ws' refers to the wind speed. The values at the bottom of each panel show the range of concentrations in the relevant percentile range. Gradient colors represent the levels of CPF probability in different percentile ranges.

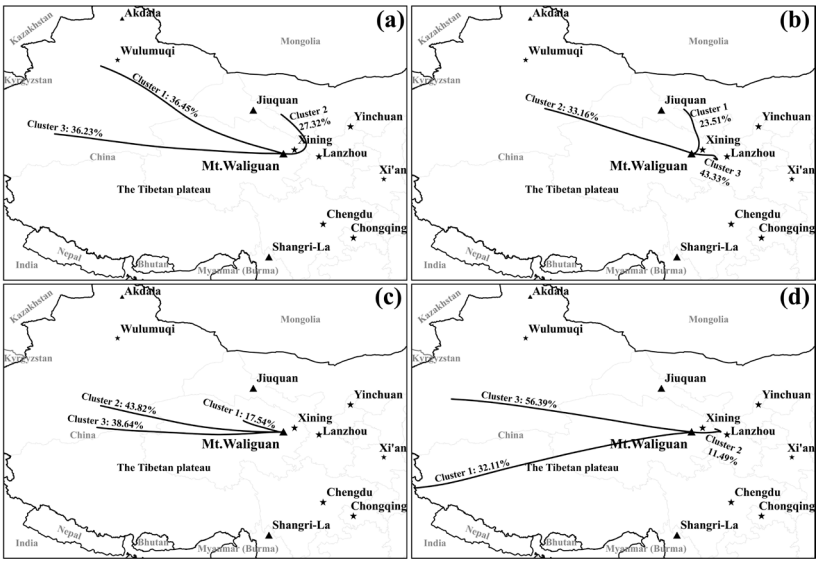

Figure 6. Cluster analysis of the 72-h back trajectories in different seasons (spring (a), summer (b), autumn (c), and winter (d)) during 2004-2019 at WLG station. The colored lines represent different clusters. The proportion of trajectories in each cluster is also marked.

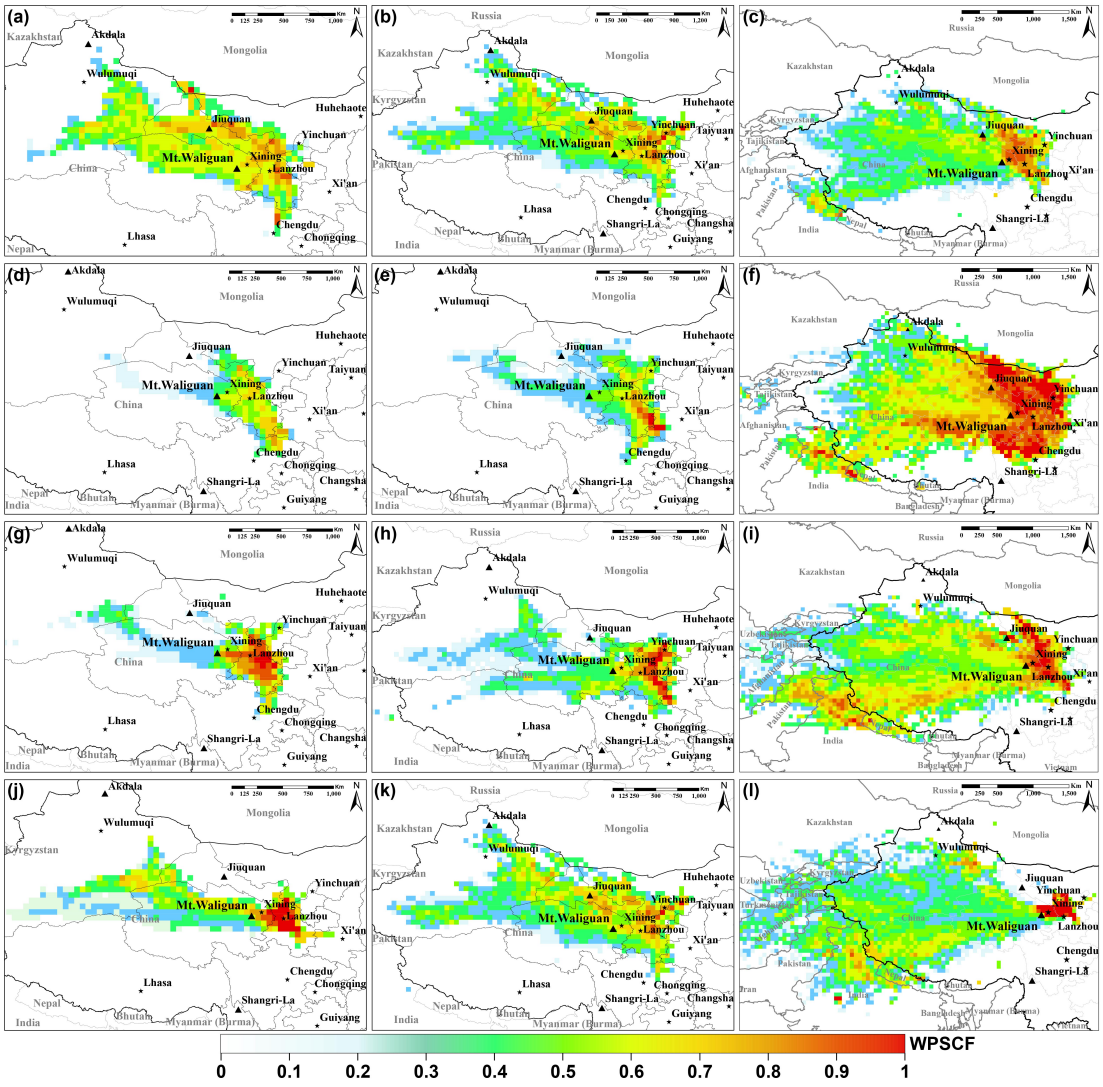

Figure 7. The geographical distribution of the weighted potential sources of CH_4 in different periods over 2004-2019 at WLG station. The gradient color shows the strong levels of potential source regions in different seasons, i.e. spring (a, b, c), summer (d, e, f), autumn (g, h, i), and winter (j, k, l), and different periods, i.e. 2004-2007 (a, d, g, j), 2008-2012 (b, e, h, k), and 2013-2019 (c, f, i, l).

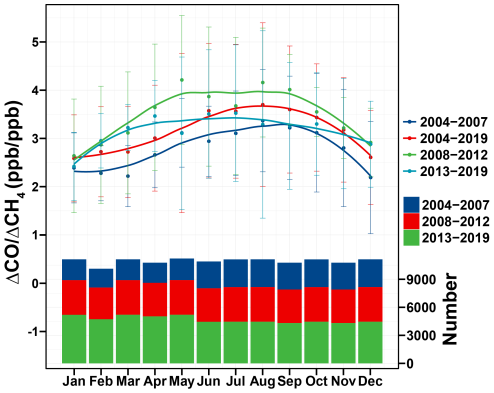

Figure 8. The average seasonal variation of the $\Delta CO/\Delta CH_4$ slopes in different periods during 2004-2019 at WLG station. The error bars show the standard deviation of the monthly averages. The lines are the smoothed curve of the averages using the method of loess (Local Polynomial Regression Fitting). The vertical bars are the monthly numbers of data in different periods.

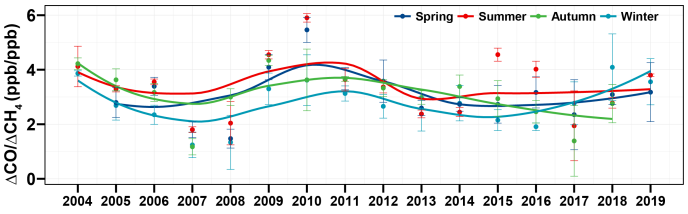

Figure 9. The long-term trend of $\Delta CO/\Delta CH_4$ slopes over 2004-2019 at WLG station. The lines are the smoothed curve of the averages using the method of loess (Local Polynomial Regression Fitting).

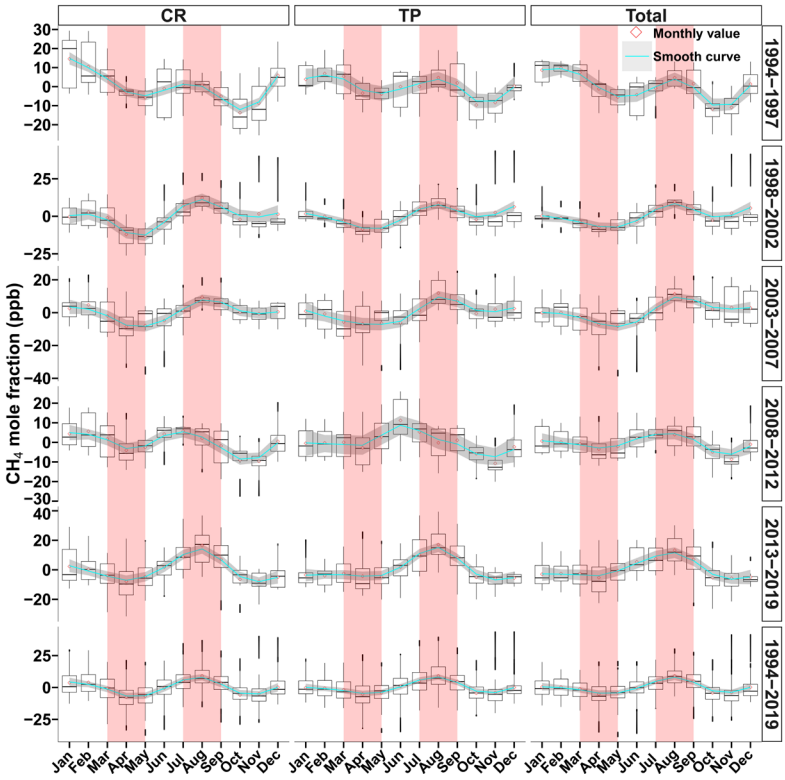

Figure 10. Monthly variations of regional CH_4 mole fractions from 1994 to 2019 at WLG station. The 'CR', 'TP' and 'Total' represent the measurements from the City Regions, the Tibetan Plateau and the total regional records, respectively. The box shows the 25th percentile, the median and the 75th percentile from bottom to top. The bottom and the top whiskers respectively reach the minimum and 1.5 times the IQR (interquartile range). The black points are identified as outliers. The red squares are the averages. The cyan lines are the smoothed curve of the averages using the method of loess (Local Polynomial Regression Fitting). The gray bands are the 95% confidence interval of smoothed curve.

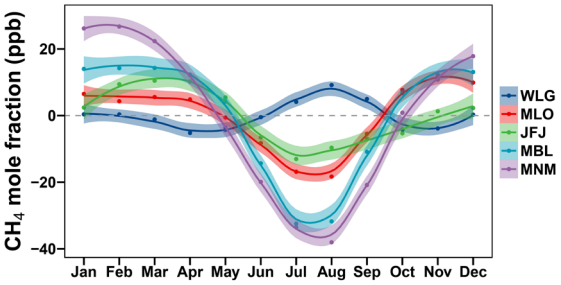

Figure 11. The seasonal cycles of atmospheric CH_4 observed at the WMO/GAW global stations of Mauna Loa (MLO, 1994-2018), Jungfraujoch (JFJ, 2005-2018), Minamitorishima (MNM, 1994-2019), and Mt. Waliguan (WLG, 1994-2019) in the Northern Hemisphere. The data of other sites (except WLG) were from WDCGG. The data in the marine boundary layer (MBL, 1994-2019) were from NOAA / ESRL lab at a similar latitude to WLG.

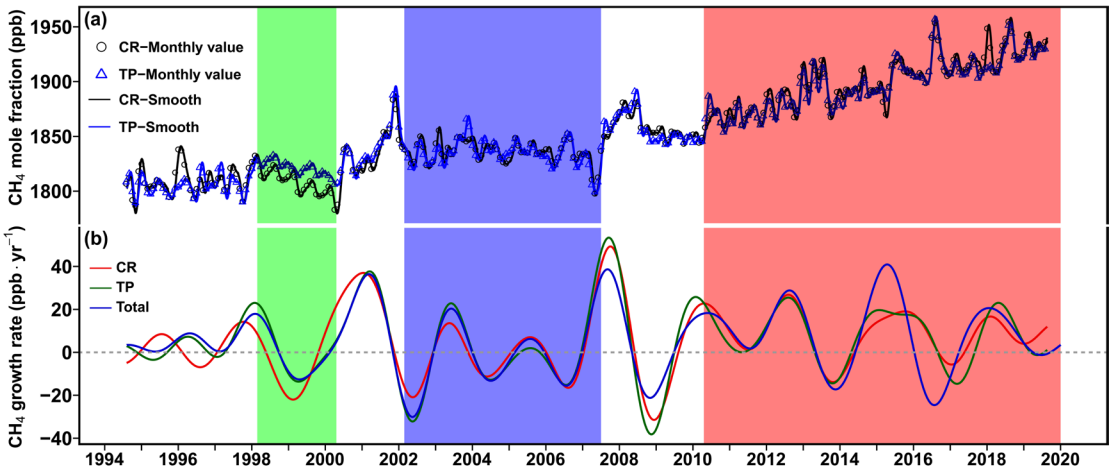

Figure 12. The top panel (a) shows the smoothed curves and monthly values of the CH_4 mole fractions in the City Regions (CR) and the Tibetan Plateau (TP) during 1994-2019 at WLG station. The bottom panel (b) is the annual growth rates of the atmospheric CH_4 records from the CR and the TP as well as the total regional time series. The growth rates were calculated from the first derivative of the trend curves. The smoothed curves and the trends were calculated using the method of Thoning et al. (1989).